Aus dem Institut für Molekulare und Verhaltensneurowissenschaften der Universität zu Köln
Direktor: Universitätsprofessor Dr. med. D. Isbrandt

Effects of the missense mutation (A263V) in the SCN2A gene on hippocampal and entorhinal cortex c-Fos expression in 7-day-old mice

Dissertation zur Erlangung der Doktorwürde
der Medizinischen Fakultät
der Universität zu Köln

vorgelegt von
Mohamad Samehni
aus Aleppo, Syrien

promoviert am 31.05.2023

Gedruckt mit Genehmigung der Medizinischen Fakultät der Universität zu Köln

Druckjahr 2023

Dekan: Universitätsprofessor Dr. med. G. R. Fink
1. Gutachter: Universitätsprofessor Dr. med. D. Isbrandt
2. Gutachter: Privatdozent Dr. med. M. B. Sommerauer

Erklärung

Ich erkläre hiermit, dass ich die vorliegende Dissertationsschrift ohne unzulässige Hilfe Dritter und ohne Benutzung anderer als der angegebenen Hilfsmittel angefertigt habe; die aus fremden Quellen direkt oder indirekt übernommenen Gedanken sind als solche kenntlich gemacht.[1]

Bei der Auswahl und Auswertung des Materials sowie bei der Herstellung des Manuskriptes habe ich keine Unterstützungsleistungen

Weitere Personen waren an der Erstellung der vorliegenden Arbeit nicht beteiligt. Insbesondere habe ich nicht die Hilfe einer Promotionsberaterin/eines Promotionsberaters in Anspruch genommen. Dritte haben von mir weder unmittelbar noch mittelbar geldwerte Leistungen für Arbeiten erhalten, die im Zusammenhang mit dem Inhalt der vorgelegten Dissertationsschrift stehen.

Die Dissertationsschrift wurde von mir bisher weder im Inland noch im Ausland in gleicher oder ähnlicher Form einer anderen Prüfungsbehörde vorgelegt.

Erklärung zur guten wissenschaftlichen Praxis:

Ich erkläre hiermit, dass ich die Ordnung zur Sicherung guter wissenschaftlicher Praxis und zum Umgang mit wissenschaftlichem Fehlverhalten (Amtliche Mitteilung der Universität zu Köln AM 132/2020) der Universität zu Köln gelesen habe und verpflichte mich hiermit, die dort genannten Vorgaben bei allen wissenschaftlichen Tätigkeiten zu beachten und umzusetzen.

Köln, den 01.10.2022

Unterschrift: …..Samehni.....

Acknowledgment

I would like to take this chance to thank all the people who supported me in finishing my doctoral thesis. First and foremost, I am honored to thank Prof. Dr. Dirk Isbrandt for giving me this opportunity to carry out my work in his lab and for having faith in my ability. I will always be grateful for his endless support, motivation, and insightful criticism, which pushed me to work harder and become a better scientist. I consider myself lucky to be supervised by such a dedicated person in the field of neurophysiology; his commitment to neuroscience has motivated me to pursue my career in this great field.

I would like especially to thank Dr. Igor Jakovcevski for being my mentor and for his endless encouragement and guidance throughout my thesis work. He was always there to answer my queries, to discuss innovative ideas and to give me his helpful feedback and expertise. He was always ready to find a solution for every problem I faced in my work in his professional calm manner. For sure I will never forget to thank Antje for her support and help with all paper works and proofreading my thesis.

I would never imagine myself being in this moment writing this thesis without the support of my mother and father who planted the love of science in my heart and lighted my way with their encouraging words. I would also never forget to send my best words of thanks to my lovely siblings Ahmad, Yaman, Hadaya, Ghufran, and Zolfa, who always put a smile on my face and gave me the power in my life.

Last, but she would never be the least, I should thank my soulmate and best friend, the mother of my wonderful children Yousef and Talia, my great wife Rima for supporting and standing beside me throughout my life, for her faith in me and for being always my motivation and inspiration to give the best of me.

Table of Contents

List of abbreviations

ABC	Avidin-biotin complex
AIS	Initial segment of the axon
BFNIS	Benign familial neonatal–infantile seizures
bp	Base pairs
BSA	Bovine serum albumin
CA	Cornu Ammonis
cAMP	3'-5'-cyclic adenosine monophosphate
CNS	Central nervous system
CREB	cAMP response element-binding protein
DAB	3,3′-Diaminobenzidine
DAPI	4',6-diamidino-2-phenylindole
DG	Dentate gyrus
dNTP	Deoxyribose nucleoside triphosphate
EC	Entorhinal cortex
EDTA	Ethylenediaminetetraacetic acid
EEG	Electroencephalography
ERK	Extracellular signal-regulated kinases
FS	Febrile seizures
GABA	Gamma-aminobutyric acid
GEFS+	Genetic epilepsy with febrile seizures plus
GFAP	Glial fibrillary acidic protein

Hcl	Hydrochloric acid
i.p.	Intraperitoneal
IBA1	Ionized calcium-binding adapter molecule 1
IEGs	Immediate early genes
IFM	Isoleucine, phenylalanine, and methionine
Ig	Immunoglobulin
LEC	Lateral entorhinal cortex
MAPK	Mitogen-activated protein kinases
MEC	Medial entorhinal cortex
NaCl	Sodium chloride
Nav1.1	Sodium voltage-gated channel alpha subunit 1
Nav1.2	Sodium voltage-gated channel alpha subunit 2
Nav1.3	Sodium voltage-gated channel alpha subunit 3
Nav1.6	Sodium voltage-gated channel alpha subunit 6
NIH	National Institutes of Health
NMDA	N-Methyl-D-aspartic acid
P	Postnatal day
PBS	Phosphate-buffered saline
PCR	Polymerase chain reaction (PCR)
PFA	Paraformaldehyde
RNA	Ribonucleic acid
RSK	Ribosomal S6 kinase

RT	Room temperature
S.E.M.	Standard error of the mean
SCN1A	Coding gene of sodium voltage-gated channel alpha subunit 1
SCN1B	Coding gene of sodium voltage-gated channel beta subunit 1
SCN2A	Coding gene of sodium voltage-gated channel alpha subunit 2
SCN2B	Coding gene of sodium voltage-gated channel beta subunit 2
SCN3A	Coding gene of sodium voltage-gated channel alpha subunit 3
SCN3B	Coding gene of sodium voltage-gated channel beta subunit 3
SCN4A	Coding gene of sodium voltage-gated channel alpha subunit 4
SCN4B	Coding gene of sodium voltage-gated channel beta subunit 4
SCN5A	Coding gene of sodium voltage-gated channel alpha subunit 5
SCN8A	Coding gene of sodium voltage-gated channel alpha subunit 8
SRF	Serum response factor
TAE	Tris-acetate-EDTA
Tris	2-Amino-2-(hydroxymethyl) propane-1,3-diol
VGSCs	Voltage-gated sodium channels

Zusammenfassung

Spannungsgesteuerte Natriumkanäle sind Transmembranproteine, die eine wichtige Rolle bei der Initiierung und Ausbreitung von Aktionspotentialen in erregbaren Zellen spielen und daher die essenziellen Vermittler der neuronalen Erregbarkeit sind. Die Dysfunktion von spannungsgesteuerten Natriumkanälen hat einen signifikanten Einfluss auf die Gehirnentwicklung und spielt eine Schlüsselrolle bei der Epileptogenese.

Die genetische Missense-Mutation im *SCN2A*-Gen (p.A263V), dass die α-Untereinheit des Natriumkanals Nav1.2 kodiert, verursacht eine neuronale Übererregbarkeit und ist mit sog. gutartigen familiären neonatalen Infantilen Anfällen als mit anderen therapieresistenten kindlichen Epilepsie-Phänotypen assoziiert.

Das Ziel dieser Studie ist die zugrunde liegenden Mechanismen der Veränderungen der Gehirnschaltkreise und das pathologische Substrat hinter den durch diese Mutation verursachten funktionellen Defiziten weiter zu charakterisieren. Ich wollte auch herausfinden, ob eine frühe postnatale Behandlung mit VGSC-Blockern die Entwicklung von Anfällen verhindern und die Mutationseffekte überwinden könnte.

Ich untersuchte die Expression von c-Fos, einem unmittelbar frühen Gen, als Marker der neuronalen Aktivierung im Hippocampus von *Scn2a* (A263V) mutierten Mäusen nach Behandlung mit Phenytoin und kontrollierte die Ergebnisse mit meinen früheren Befunden von nicht behandelten Mäusen. Ich habe auch die Expression von c-Fos im entorhinalen Kortex von mutierten Mäusen untersucht, um herauszufinden, ob es eine Zunahme der neuronalen Aktivierung als erwartete Ausbreitungsregion der neuronalen Übererregbarkeit gibt.

Meine Ergebnisse zeigten eine Abnahme der neuronalen Aktivierung im Hippocampus von 7 Tage alten mutierten Mäusen nach der Behandlung mit Phenytoin, wie durch eine geringere c-Fos-Expression sowohl in heterozygoten als auch in homozygoten mutierten Mäusen gezeigt wurde.

Zusammengenommen konnten die mutierten Mäuse zwar nach der Behandlung mit Phenytoin nicht überleben, aber meine Ergebnisse zeigten eine effiziente Unterdrückung der durch Mutationen ausgelösten neuronalen Übererregbarkeit im Hippocampus, dem erwarteten Ursprung von Anfällen bei *Scn2a* (A263V) mutierten Mäusen. Diese Studie bildet die Grundlage für zukünftige Analysen, die darauf abzielen zu untersuchen, ob übererregbare neuronale Schaltkreise in Mäusen mit *Scn2a* (A263V)-Mutation zu Neurodegeneration und Zellverlust führen, und für weitere Behandlungsstudien.

Abstract

Voltage-gated sodium channels are transmembrane proteins that play a vital role in the initiation and propagation of action potentials in excitable cells and are the essential mediators of neuronal excitability. Dysfunction of voltage-gated sodium channels significantly affects brain development and plays a critical role in epileptogenesis.

A genetic missense mutation in the *SCN2A* gene (A263V), which encodes the α-subunit of the sodium channel Nav1.2, has been documented to cause neuronal hyperexcitability and to associate with benign familial neonatal infantile seizures and other therapy-resistant childhood epilepsy phenotypes.

In this study, I aimed to characterize further the underlying mechanisms of brain circuitry alterations and the pathological substrate behind functional deficits caused by this mutation. I also aimed to find out if early postnatal treatment with a VGSC blocker could prevent the development of seizures and overcome the mutation effects.

I studied the expression of *c-Fos*, an immediate early gene, as a marker of neuronal activation in the Hippocampus of *Scn2a* (A263V) mutant mice after treatment with phenytoin and controlled the results with my previous findings of not-treated ones. I also investigated the expression of *c-Fos* in the entorhinal cortex of mutant mice to determine if there was an increase in neuronal activation as an expected propagation region of neuronal hyperexcitability.

My results showed decreased neuronal activation in the hippocampus of 7-day-old mutant mice after treatment with phenytoin, as demonstrated by lower c-Fos expression in both heterozygous and homozygous mutant mice.

Taken together, even though prolonged treatment with phenytoin resulted in increased mortality in mutant mice, my results showed an efficient suppression of the mutation-triggered neuronal hyperexcitability at the hippocampus, the proposed origin of seizures in *Scn2a* (A263V) mutant mice. This study provides the basis for future analyses to investigate whether hyperexcitable neural circuitry in *Scn2a* (A263V) mutant mice leads to neurodegeneration and cell loss and for further treatment studies.

Introduction

Epilepsy and seizures

Epilepsy is a chronic condition characterized by recurrent seizures, accompanied by neurobiological, psychological, and cognitive disorders, which could be triggered by many different factors[1].

About 1% of the general population and around 70 million people in the world has a form of epilepsy[2] with an incidence of 50 new cases per 100,000 people each year, and for children under two years, it is more than 70 cases per year[3]. Thus, epilepsy is considered one of the most frequent neurological disorders [4]. Since 2014, it has been considered a disease and no longer a disorder[5].

It is classified as focal epilepsy when the seizure activity begins in one hemisphere and as generalized if it arises in both hemispheres. When it is neither focal nor generalized, it would be classified as unknown[1,6].

More than 75% of all epilepsy cases start during childhood, a period of intense brain development in which even the healthy brain is susceptible and prone to seizures, probably because inhibitory neuronal circuits develop later than the excitatory circuits[1,7]. In addition, gamma-aminobutyric acid (GABA), the main inhibitory neurotransmitter in the brain, may have a depolarizing or even excitatory action in the fetal and early childhood phases[8].

Numerous studies indicate that genetic or acquired factors can disturb brain function at many diverse levels and affect synaptic connectivity, receptors, and ion channel function, ultimately altering the excitation/inhibition balance in neuronal circuits. An imbalance between excitation and inhibition in neuronal circuits makes the brain seizure-prone[3]. A seizure is an excessive, abnormal, self-limited, and hypersynchronized electrical activity of the neurons in the brain, with a wide range of genetic and acquired etiologic triggers and risk factors. [9] When a seizure persists for more than 30 minutes, it is called status epilepticus [10].

An epileptic seizure is the term coined to describe seizures caused by an epilepsy condition in order to distinguish them from other seizures, which could be triggered by reversible brain injuries (e.g., fever, hypoglycemia) or by a psychogenic state[1,11]

Etiology of epilepsy

It is fundamental to understand the etiologies of epilepsy to conduct an effective therapy. They can be defined in six etiologic categories (genetic, structural, infectious, metabolic, immune, and unknown)[5,9].

Brain tumors are manifested in up to 30% of epilepsy, particularly when the tumor is located in the temporal lobe or near the central sulcus[2,9,12]. Moreover, in patients with severe brain trauma, there is a sevenfold risk of epilepsy as compared to people without brain injury. On the other hand, about 4% of epilepsy cases are due to the presence of a tumor[9].

Furthermore, infection with the herpes simplex virus, which causes herpes simplex encephalitis, is correlated with a higher risk of developing epileptic seizures[13].

Genetic epilepsy

It is assumed that 16 different genetic factors contribute to more than 30% of all epilepsy cases, with 977 genes confirmed to be associated with epilepsy conditions. A higher rate of epilepsy incidence among monozygotic compared with dizygotic twins has been shown[14]. The most prominent genetic disorders are mutations of neuronal ion channels, which have implications for the balance of neuronal excitatory and inhibitory functions, developmental abnormalities, and neuronal death[3,15].

The age of onset and severity of genetic epilepsy depends on the functional and structural consequences of pathogenic sequence variants or chromosomal abnormalities and their importance for neuronal network development and homeostasis[16].

Ion channels

Ion channels are membrane pore-forming proteins that play a vital role in neuronal signaling. By regulating the passage of ions between both sides of the cell membrane, they control the generation and propagation of action potentials and regulate the resting membrane potential[17]. Based on their gating properties, i.e., what opens and closes a channel, they can be divided into ligand-dependent, voltage-dependent channels, essential for synaptic transmission, ATP-gated (K-ATP), stretch-activated, Ca-activated, pH-activated, and mixed types. There are voltage-dependent channels for calcium, potassium, chloride, and sodium ions[17].

Voltage-gated sodium channels (VGSCs)

Voltage-gated sodium channels (VGSCs) are transmembrane proteins that open in response to depolarizing changes in the membrane potential and inactivate spontaneously within milliseconds[18]. They play an essential role in the initiation and propagation of action potentials in excitable cells such as neurons, myocytes, and endocrine cells[13].

Structure of voltage-gated sodium channels (VGSCs)

Voltage-gated sodium channels have three subunits: one pore-forming α subunit of about 260 kDa and two 33-36 kDa β subunits[17,19]. There are four types of β subunits in the adult brain: SCN1B, SCN2B, SCN3B, and SCN4B with a broad distribution across brain regions[20]. Sodium channel α-subunits have different kinetic and voltage properties depending on the tissue. They are made of four domains (DI–IV), and each domain has a structure that consists of six transmembrane segments (S1–6). In total, each domain has approximately 2,000 amino acid residues[20]. The voltage-sensing mechanism, an essential player in the activation of the channel, is contained in the fourth segment of each domain, whereas the channel inactivation machinery is thought to be contained in the linker between DIII and DIV, which has an IFM (isoleucine, phenylalanine, and methionine) motif[21,22]. Voltage-gated sodium channel α-subunits show significant homology with calcium and potassium voltage-gated channel α subunits[23]. The β subunits are essential channel function modifiers, and they are believed to have a critical role in cell adhesion, initiation of contacts with extracellular matrix proteins, and gating[23]. Therefore, sodium channel β subunits essentially contribute to controlling the excitability of neurons[17,24].

Neurobiology of voltage-gated sodium channels (VGSCs)

After stimulation of the membrane by synaptic transmission, a slight membrane depolarization takes place and VGSCs open up, leading to inward sodium flow causing fast depolarization of the membrane potential and initiation of an action potential, followed by fast channel inactivation that stops the sodium flux across the membrane[21]. Then the voltage-gated sodium channels go to a resting state, at which point they cannot open, or be activated again (refractory period), until the voltage-gated potassium channels open up and repolarize the membrane.

Expression of voltage-gated sodium channels (VGSCs)

There are nine identified VGSC α subunit genes in the human genome, each with a specific pattern of expression in the brain and distinct functions. In the etiology of genetic epilepsy, different VGSC genes have been implicated: *SCN1A, SCN2A, SCN3A*, and *SCN8A* each code for a channel protein: Nav1.1, Nav1.2, Nav1.3, Nav1.6, respectively[22] and *SCN1B* (encoding Navb1)[17]. Nav1.2 is mainly expressed in axonal terminals and axons[25] and is strongly associated with benign familial neonatal-infantile seizures[26]. During development, the expression of various VGSC subunits has different levels. For example, *SCN3A* mRNA has a higher expression level in neonatal brains, suggesting an essential role in development, whereas *SCN1A, SCN2A*, and *SCN8A* mRNAs have higher expression levels in the adult brain emphasizing their vital role in adult brain function[22]. *SCN2A* expression is age and brain region specific.

SCN2A and SCN8A are the main VGSCs subtypes expressed in the excitatory neurons. Neurons with a low action potential threshold express mainly SCN8A channels, whereas neurons with a high action potential threshold express mainly SCN2A channels[27]. SCN2A channels are predominant in the unmyelinated axons, especially in the initial segment of the axon (AIS), which is the neuronal site of action potential initiation and is considered important for genetic epilepsies[22,28,29]. The proximal part of AIS has high levels of Nav1.2 channels (Sodium voltage-gated channel alpha subunit 2), whereas the distal part of AIS has high levels of Nav1.6 channels[22].

Electrophysiological studies indicate that action potential initiation takes place at the distal part of the initial segment of the axon, as it has a low threshold property, whereas backpropagation of the action potentials to the soma and dendrites occurs at the proximal part of the initial segment of the axon, as it has a high threshold property[27,30].

Developmental changes in Nav1.2 expression

Nav1.2 channels are highly expressed in the hippocampus, cortex, midbrain, and striatum[29]. During development, Nav1.2 is expressed in two different splice isoforms, a neonatal and an adult form with reported differences in the gating properties. This developmental change in SCN2A expression is paralleled by functional changes as a result of alternating 5A and 5N coding exons. The 5A isoform with a neutral amino acid residue, which is highly expressed during the first two weeks of life, is more excitable than the 5N isoform that contains an aspartic acid residue[31,32]. Other studies show that exon 5N/5A ratio in the mouse brain is region

dependent, with a high level in the cortex and hippocampus, and age related, since the expression level of 5N decreases significantly during the first weeks of life[22].

The neonatal splice variant has less excitability compared to adult isoform at similar expression levels. It shows a depolarizing shift of the voltage dependence of activation, a hyperpolarizing shift of the voltage dependence of fast inactivation, a faster time course, and slower recovery from fast inactivation, which could explain the pathogenicity of SCN2A during the neonatal period[17,32,33].

On the other hand, SCN2A subunits have during the first two weeks of life high expression levels in the hippocampus and cortex[34]. Later, they are only highly expressed in specific structures, such as in unmyelinated mossy fibers and in the axons of CA1, CA3 pyramidal cells in the hippocampus, and parallel fibers in the cerebellum.

Remarkably, high expression levels of Nav1.2 have been reported in excitatory pyramidal neurons as well as in the inhibitory neurons especially of somatostatin-positive, reelin-positive/somatostatin-negative and vasoactive intestinal peptide-positive, but not parvalbumin-positive interneurons[33,35].

Mutations of voltage-gated sodium channels (VGSCs)

Voltage-gated sodium channels have a very low rate of coding variation and belong to the 2% most conserved proteins in the human genome, with an estimation of 5% of epileptic encephalopathies[36,37].

More than 900-point mutations of Nav channels have been identified in the central and peripheral nervous system, heart, skeletal muscles, and cancer cells[38].

It has been shown that mutations in VGSCs are associated with neuronal hypo- or hyper-excitability, with a wide disease's spectrum such as epilepsy, migraine, pain, autism, cardiovascular diseases, and diabetes[22,38].

A wide spectrum of genetic epilepsy syndromes has been linked to VGSC mutations; most of these syndromes include generalized seizures (Figure 1).

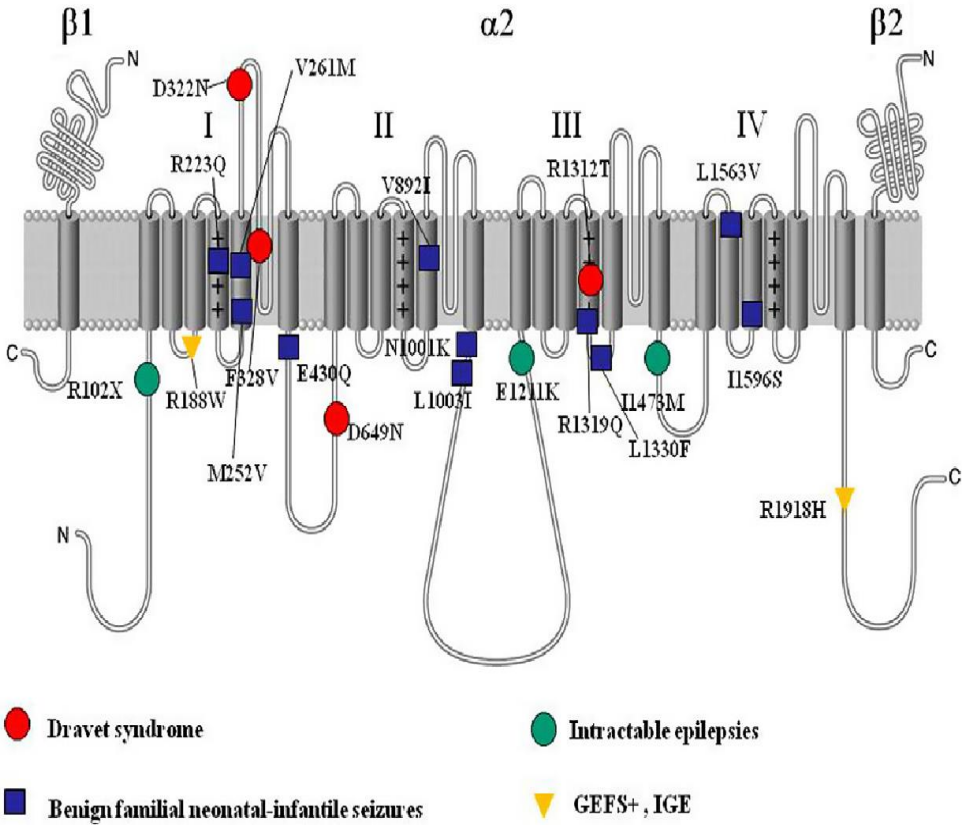

Figure 1| ***Clinical spectrum of SCN2A mutations in epilepsy.*** Red circles refer to mutations identified in Dravet syndrome, blue squares refer to mutations causing benign familial infantile seizure, green circles refer to mutations causing intractable epileptic encephalopathy, and yellow triangles refer to mutations causing febrile and afebrile seizures[23].

The *SCN1A* gene, which is located at the 2q24.3 chromosome and expressed predominantly in inhibitory GABAergic interneurons, is considered as one of the most frequent targets of mutations in genetic epilepsy syndromes causing generalized epilepsy with febrile seizures plus, type 2 (GEFS+2, MIM 604403)[39], familial febrile seizures (MIM 604403), familial hemiplegic migraine (MIM 609634), and to cause early infantile epileptic encephalopathy (Dravet syndrome, MIM 607208)[36].

SCN4A and SCN5A are widely expressed in human skeletal and cardiac muscles, respectively. Mutation of *SCN4A* is associated with periodic paralysis, whereas mutations in *SCN5A* are linked to long QT syndrome[18] A *SCN8A* mutation in a patient with severe infantile encephalopathy at the age of 6 months was confirmed and resulted in the unexpected death at the age of 15 years[40], also it was confirmed that mutations of *SCN8A* cause benign familial

infantile seizures (MIM 617080) and cognitive impairment with or without cerebellar ataxia (MIM 614306)[36].

Phenotypic spectrum of *SCN2A* gene mutations

Mutations of the *SCN2A* gene, which is located at chromosome 2q24.3, the same gene cluster harboring the *SCN1A-SCN3A* genes[36], are associated with a wide range of neurodevelopmental phenotypes and play a leading role in genetic epilepsy since SCN2A is the main subunit at the AIS and expressed especially in the excitatory, glutamatergic neurons[41,42].

Despite a high degree of phenotypic variability, a relationship between the phenotype of the patients with SCN2A mutations and the underlying functional alterations has been well identified.

SCN2A mutations can be categorized in:

- gain of function which causes neuronal hyperexcitability which is mainly correlated with epilepsy with onset before age of 3 months and well treated with sodium channel blockers (SCBs).
- loss of function which is associated with autism and intellectual disability; however, some studies have identified loss of function linked to late-onset epilepsy; after the age of three months; with unclear mechanisms and bad or no response to SCBs[33,36].

More than 100 SCN2A variants have been identified in patients with benign familial neonatal–infantile seizures (BFNIS), generalized epilepsy with febrile seizures plus (GEFS+), Dravet syndrome, West syndrome, epilepsy of infancy with migrating focal seizures and some intractable childhood epilepsies phenotypes[36,43]. Movement disorders chorea and episodic ataxia were also described by patients with SCN2A Mutations[44].

Most of these mutations are missense mutations, and recently one nonsense mutation was identified in a case with intractable childhood epilepsy[23].

GEFS+ is an autosomal dominant syndrome associated with generalized epilepsy phenotypes. It is a clinical phenotype of febrile seizures (FS) with frequent episodes beyond six years of age (FS+)[23]. Febrile seizures associated with afebrile seizures were reported in patients with a SCN2A missense mutation (R187W), which causes slow inactivation of the mutant channel and neuronal hyperexcitability[45].

Benign familial neonatal infantile seizures are present in autosomal dominant pedigrees associated with (M252V, V261M, R1319Q, L1330F, and L1563V) SCN2A missense and mainly gain of function mutations[23,34,44,46], with substitutions between physicochemically similar amino acids which could explain the mild manifestation of the disease[47].

Clinically, they manifest as seizures in neonates ages, ranging from 1 day to 23 months[44]. As the children develop, they normally outgrow the epileptic seizures and get better, ultimately entering full remission normally by the age of 5 years[26,48]. This transient and self-limiting course of disease with no neurodevelopmental disability is the most common one associated with SCN2A missense mutations[23] and could be explained by the reorganization of the initial segment of the axon during brain development. In this case, SCN2A in the distal AIS is replaced by SCN8A, leading to a decreased effect of mutant SCN2A[34].

Despite benign familial neonatal infantile seizures having autosomal inherited genetics in up to 82%, seizure semiology shows a wide variation, especially in seizure treatment response. Some cases were reported to be resistant to antiepileptics drugs AEDs, particularly in de novo cases; in these sodium channel blockers (phenytoin, oxcarbazepine, and carbamazepine) showed a good control over the seizures[44].

On the other hand, some SCN2A mutations in early neonatal ages were manifested as an epileptic syndrome with severe epilepsy and neurodevelopmental disability like Ohtahara syndrome (OS) and epilepsy with migrating focal seizures of infancy (EIMFS [44]).

Ohtahara syndrome manifests as tonic seizures or spasms with a burst-suppression pattern in EEG, whereas epilepsy with migrating focal seizures of infancy (EIMFS) shows variant types of focal seizures accompanied by clinical or EEG evidence of seizure migration from one hemisphere to the other. Both syndromes are drug resistant but seizure control and in some cases seizure freedom with a diminishing of the burst-suppression pattern in EEG was described by using phenytoin[44,49].

Another severe SCN2A-related epileptic syndrome with cognitive disability and drug resistance but with a late infantile-onset is West Syndrome and its wide range of epileptic manifestations and an evolving possibility into Lennox-Gastaut syndrome[44].

A de novo missense mutation of SCN2A (R1312T) has been identified in a patient with Dravet syndrome, which is a malignant epilepsy syndrome with an onset in the first year of life with prolonged seizures and sudden unexpected death in epilepsy (SUDEP)[23,50].

Remarkably, the majority of late-onset SCN2A related epilepsy syndromes are mainly due to de novo loss-of-function missense mutations with substitutions between physicochemically dissimilar amino acids which could explain the severe manifestation of the disease. In addition, sodium channel blockers including phenytoin in comparison with early infantile onset epilepsy syndromes were mostly not effective and in up to 25% of cases induced an exacerbation of seizures, which could be understood by taking in account the expected decrease in SCN2A-channel availability and membrane excitability by loss-of-function mutations[44].

In contrast to missense mutations, truncating and nonsense variants were mainly observed in patients with autistic symptoms or developmental retardation and only in late-onset epileptic syndromes[44].

Bartnik and colleagues proposed that inactivating loss of function mutations or deletion copy number variations of SCN2A gene will cause haploinsufficiency of SCN2A and could be responsible for severe psychiatric phenotype abnormalities accompanied by epilepsy[51]. Growing evidence suggesting the role of SCN2A loss-of-function mutations in schizophrenia has been reported[52,53].

Clinical manifestation of patients with the *SCN2A* (p. Ala263Val) gene mutation

The SCN2A gain-of-function (p.Ala263Val) mutation disturbs a highly conserved amino acid in Nav1.2 and leads to neonatal onset of neuronal hyperexcitability by slowing the inactivation time course due to a depolarizing shift in which more channels are available for activation at resting membrane potential, and on the other hand, increasing the persistent sodium current which in turn causes a depolarization of neurons membrane leading to synaptic potentials amplification and subthreshold oscillations generation[23,33,46].

A patient with the SCN2A (p.A263V) missense mutation was reported to have neonatal-onset seizures with late onset, after 18 months of age, episodes of ataxia, myoclonia, headache, hypermotor activity, hyperventilation, retching or vomiting, and back pain[46].

Another group has reported an Ohtahara syndrome caused by SCN2A (p.A263V) mutation, which indicates a phenotypic pleiotropy of this mutation[54].

The hippocampus and its contribution to epilepsy

The hippocampus is an important part of the limbic system in the human and mammalian brains, which is located in the temporal lobe under the cerebral neocortex[55]. It originates from the telencephalon and consists of the dentate gyrus (DG) and the cornu Ammonis (CA), which

is subdivided into the CA1, CA2, and CA3 subfields[55] (Figure 2). It plays an essential role in episodic memory formation and retrieval, spatial orientation, and in different pathological conditions, such as epilepsy and Alzheimer's disease[56,57]. The hippocampus consists of a heterogeneous neuron population, which is distinguished by their connectivity and morphological characteristics. Neurogenesis in the mammalian hippocampus, a formation of new neurons, dendrites and synapses, and continuous reorganization, appear to play a significant role in the hippocampal plasticity during postnatal periods and persist during the entire lifespan[58]. The hippocampus proper, dentate gyrus, and CA fields, with the subiculum, presubiculum, parasubiculum, and entorhinal cortex are called the hippocampal formation, which has a unique connectivity pattern called trisynaptic circuit[56].

In this circuit, sensory input from the upper layers of the entorhinal cortex is transferred to the DG and CA3 through the perforant pathway and then through the mossy fibers from the DG to the pyramidal cells in CA3[59,60], which in turn transmits the input via Schaffer collaterals to CA1[61]. Through the projections of CA1 pyramidal layers, the information is transmitted to the subiculum and further to deep layers of the entorhinal cortex [56].

SCN2A mutation-triggered epilepsy could be explained by pathological alteration of feedforward in these synaptic circuits due to hyperexcitability of the excitatory neurons or inhibition reduction in the CA3 region[33]

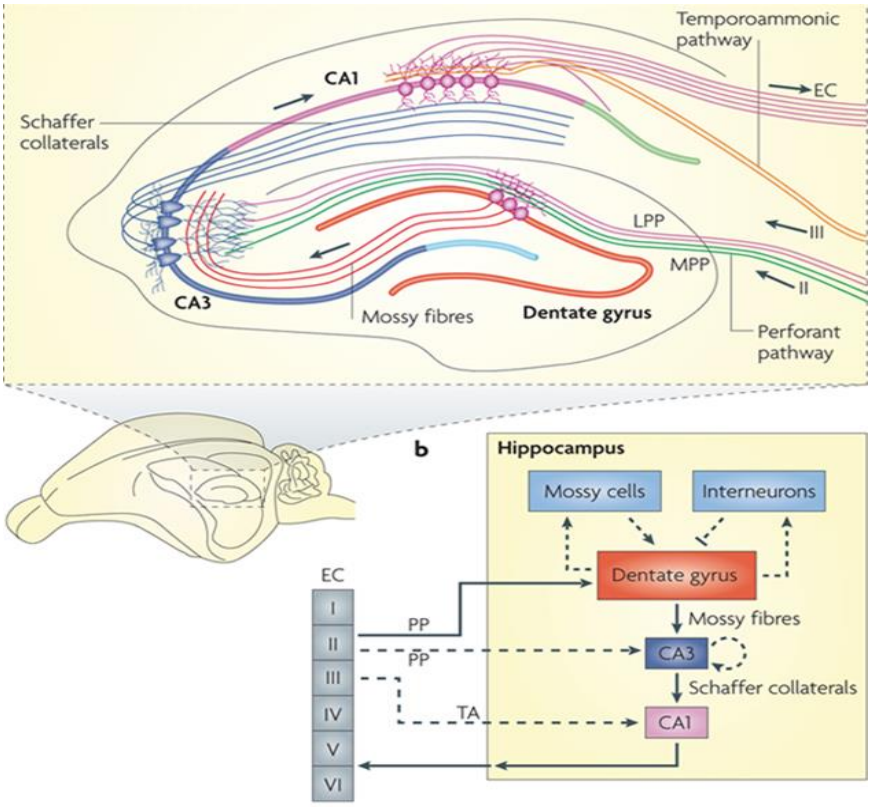

Figure 2| ***Schematic illustration of the hippocampal structure and its connectivity pathway tri-synaptic-circuit***[106].

C-Fos and related immediate early genes as markers of neuronal activity

Immediate early genes (IEGs) are rapidly activated genes that are expressed for transient periods in response to different types of physiological and pathological cellular stimuli such as growth factors, neurotransmitters, and sensory stimulation. Their expression can be used as an instrumental marker of cell activation to anatomically map the functional cells in different brain and neuroendocrine system regions since this expression cannot be prevented by protein synthesis inhibitors[62,63]. After stimulation of an immediate early gene, it encodes a transcription factor that affects and interferes with the expression of target genes. These target genes in turn mediate extracellular signaling and modulate a long-term cellular phenotype (Figure 3)[63,64]. The best-characterized immediate early gene-encoded transcription factor is c-Fos. Advantages of c-Fos as a marker over other IEGs are

- Its ability to be activated by a wide range of transsynaptic stimuli.
- Very low expression levels under basal conditions.
- Ease of detection.

- Its sensitivity after neuronal activation.
- Cellular mapping.
- The possibility of the detection of neurons in a certain network in different brain regions.
- The possibility of combined c-Fos staining with other immunohistochemical markers [65].

However, c-Fos has some limitations, for example that not all activated neurons express c-Fos, that it can detect only activated neurons, but not inhibited ones, that it cannot differentiate short-lasting from long-lasting neuron activity, and that it is only possible to analyze information from a single time point in each animal[65,66].

Despite these limitations, it is still the most commonly used technique for detecting and analyzing neuronal activation. A few minutes after stimulation, transcription of c-Fos starts and it reaches its expression peak after 30 to 60 min. Subsequently, it is gradually degraded to its basal level with a half-life of minutes to an hour after the activating stimulus ended [64]. It was thought that the c-Fos level of activation indicated the neuronal functional activity and that it was synaptogenesis and differentiation related, but it has been shown that some brain areas with high neuronal activity levels do not have high c-Fos expression under basal conditions, which has been explained by a difference in activation threshold among different regions of the brain[64].

The molecular mechanism that causes c-Fos activation is depicted in (Figure 3). Furthermore, it has been shown that the expression of c-Fos in the brain is region- and age related. During development, high expression levels of c-Fos mRNA have been identified in the rat brain between postnatal days P0 and P16. Beyond this age, the expression level decreased and, by age of P30, only low levels of c-Fos mRNA were identified in the hippocampus and striatum[64].

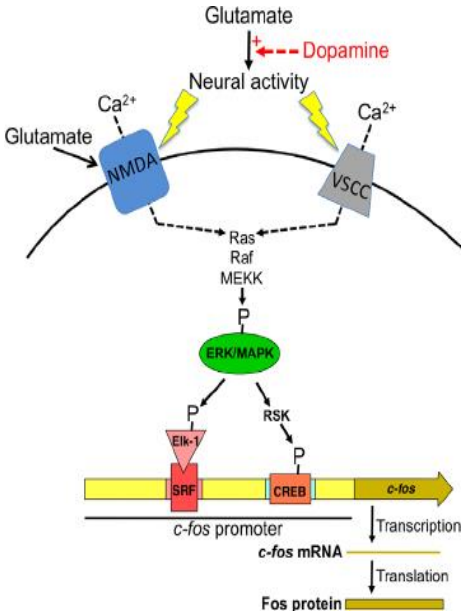

Figure *3* ***Illustration of the molecular mechanisms of c-Fos and Fos expression in activated neurons***. Dopamine improves glutamate-mediated neural activation which triggers calcium (Ca2+) influx through NMDA-type glutamate receptors and voltage-sensitive calcium channels to phosphorylate and activate ERK/MAPK via the Ras-Raf-MEKK pathway. Activation of ERK/MAPK causes a phosphorylation of Elk-1 which is associated with serum response factor (SRF) in addition to phosphorylation of CREB via ribosomal S6 kinase (RSK). Phosphorylation of transcription factors Elk-1/SRF and CREB can start transcription of the coding sequence for c-Fos[58].

Generation of *Scn2a* (p. Ala263Val) gene mutant mouse

The mutant mouse line was generated in the laboratory of Prof. Isbrandt to study developmental epileptogenesis in sodium channelopathy. Mice heterozygous for the mutation were also used to study the effect of increased neuronal sodium influx on inflammation-derived axonal injury in an experimental autoimmune encephalitis (EAE) model (Figure 4)[67]. The authors reported that heterozygous mutant mice had increased neuronal degeneration and elevated disability and lethality following CNS inflammation in comparison with their wild-type littermate controls. Despite CNS inflammation, there was no apparent difference in immune cell infiltration. Previous work in the laboratory of Prof. Isbrandt on the *Scn2a* (A263V) mutant mouse model showed reduced body weight and altered behavior accompanied by signs of hyperexcitability and electrophysiological abnormalities in the hippocampus region of homo- and heterozygous mutants, starting from neonatal age (P7), while motor seizures were only

observed from P15 onward in homozygous mutant mice. At later ages (between 3 and 6 weeks), the mice exhibited increased motor activity, cognitive impairment, and developed spontaneous and sometimes lethal epileptic seizures. Early postnatal treatment with the VGSC blocker phenytoin prevented the development of seizures in a pilot study (Sarah Schöb and Walid Fazeli, personal).

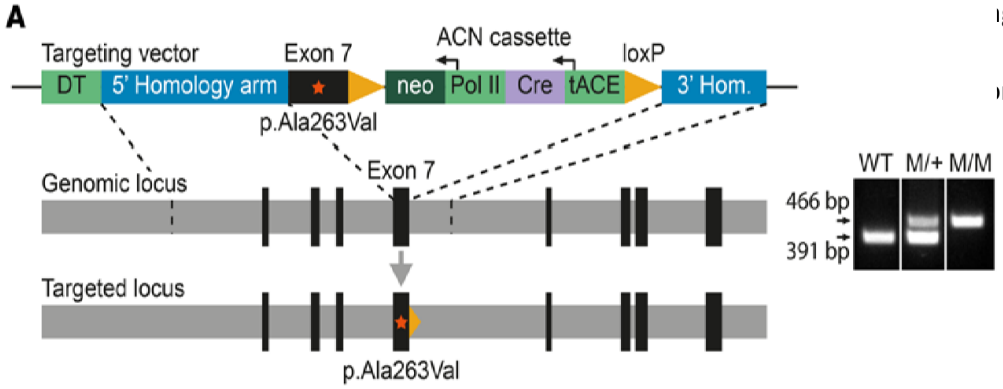

Figure 4| ***Scn2a (A263V) mouse line generation.*** A schematic illustration of targeting strategy of knock-in mice carrying the human p.Ala263Val gain-of-function mutation in the *SCN2A* gene, and an image representative of PCR genotyping of wild-type, heterozygous (M/+), and homozygous (M/M) knock-in animals[67].

Management of early epilepsy

In up to 30% of children with epilepsy, they will need two or more antiepileptic drugs (AEDs) to control seizures with many side effects from medication. A consideration of dietary therapy, resistive epilepsy surgery, stimulation techniques or palliative care could be taken in those who don't respond enough to AEDs[68].

Interestingly, Antiepileptic drug (AED) therapy reduces seizure recurrence risk, but the question is if it does alter the underlying disease process.

Antiepileptic therapy in SCN2A-related epilepsy and Voltage-gated Sodium Channel Blockers

Antiepileptic therapy in neonates has not changed during the last 10 years. The traditional broad-spectrum antiepileptic sodium channel blockers (SCBs) especially carbamazepine (CBZ) and phenytoin (PHT), which bind preferentially to the inactivated states of Nav channel, are still the first-line treatment of neonatal seizures, particularly those related to gain-of-function mutations in VGS channel[69].

An important limitation of the clinically used SCBs is, that they are nonselective which makes it practically difficult to sufficiently saturate the binding sites in sodium channels with the clinically used dosage[70].

Phenytoin stabilizes sodium channels and reduces electrolyte exchange across the membrane and is considered the first line in the treatment of SCN2A Mutation. Despite its broad-spectrum and potent antiepileptic effects, it has some disadvantages. It is 95% metabolized by the liver, protein bound, its plasma concentration is affected by both enzyme-inhibiting and enzyme-inducing drugs and induces irritation at the injection site. In addition, it shows a first-order reaction at low plasma concentrations and zero order at high concentrations, which makes it difficult to decide the optimal dosage in neonates[71].

Furthermore, to control seizures completely a high dosage of phenytoin is needed, which is hard to establish due to its kinetics profile[44].

My previous Work

It has been confirmed that the hippocampal region and its connectivity networks play an essential role in epileptogenesis, and for this reason, my work on the Nav1.2 epilepsy mouse model was focused on the hippocampal structures as a possible area of origin of the seizures[72].

Body weight of neonatal *Scn2a* (A263V) mutant mice compared with matched wild-type control

I analyzed the body weight of the P7 *Scn2a* (A263V) mutant mice as a sensitive indicator of developmental alterations that could be triggered by genetic mutations. The body weight of homozygous *Scn2a* (A263V) mutant mice was significantly decreased compared to their matched wild-type controls and to the heterozygous mutant mice. On the other hand, the *Scn2a* (A263V) heterozygous mutant mice exhibited no significant difference in their body weight in comparison with their matched wild-type controls.

Thickness of hippocampal structures

In order to exclude the effect of layers' thickness on the density of the counted cells, I calculated the thickness of hippocampal structures using Nissl fluorescent staining[73]. There was no significant difference in the thickness of the hippocampal layers between the *Scn2a* (A263V) mutant, heterozygous mice, and wild-type mice.

Neuronal network activity in the hippocampus region

As seizures result in hypersynchronized neuronal activity, I investigated whether the mutation in Nav1.2 led to neuronal network hyperactivity in the hippocampal region by quantifying the nuclear immunohistochemical staining for the c-FOS transcription factor since c-*Fos* is one of IEGs with a low expression level under basal conditions[64] and provides an indication of recent neuronal activity[75]. for the estimation of the profile density of activated neurons (i.e., the number of stained nuclei in a specific measured area).

In 7-day-old mice, the number of neurons expressing nuclear c-FOS immunoreactivity in each structure of the hippocampus (CA1, CA3, and DG) was significantly higher in homozygous *Scn2a* (A263V) mutant mice as compared to their wild-type littermates. Similarly, the number of c-FOS-immunoreactive neurons in all hippocampal structures (CA1, CA3, and DG) of heterozygous *Scn2a* (A263V) mutant mice was also significantly higher as compared to their

wild-type littermates. Interestingly, there was a significant difference between heterozygous and homozygous mutant mice. Consequently, we can conclude that the A263V mutation in Nav1.2 has an important effect on the neuronal hippocampal activity and causes neuronal hyperactivation in a gene dose-dependent manner.

Aim of the study

To further understand the underlying mechanisms of brain circuitry alterations and the pathological substrate behind functional deficits caused by the *Scn2a*(A263V) mutation, the following specific questions were raised:

- Whether early postnatal treatment with the VGSC blocker phenytoin prevents the development of seizures and reduces neuronal activation, measured by c-Fos expression in 7-day-old *Scn2a* (A263V) mutant mice.

- Is there increased neuronal activation in the entorhinal cortex, measured by c-Fos expression, in 7- day-old *Scn2a* (A263V) mutant mice.

To answer these questions, I studied the morphology of *Scn2a* (A263V) mutant mice brain and compared it to their littermates after treatment with phenytoin using quantitative morphological methods combined with light microscopy.

First, I examined whether the increased excitability of neurons due to an SCN2A mutation could be reversed by phenytoin treatment in mutant mice for a period of seven days starting at P1. This was accomplished by using c-Fos immunoreactivity as a marker of network hyperactivity, which provides an indirect measure of recent neuronal activity[75]. At P7, the number of c-Fos–immunoreactive neurons was counted in the hippocampus of mutant mice, in a region- and layer-specific manner (CA1, CA3 layers and the dentate gyrus), with and without phenytoin treatment. In addition, several cortical regions, including the entorhinal cortex, which has strong connectivity with the hippocampus, were examined.

Moreover, I investigated whether the increased excitability of neurons due to an SCN2A mutation leads to neuronal dispersion and cell loss in the entorhinal cortex in P7 mice.

Brains of P7 SCN2A mutant mice and their wild-type littermates for my experiments were collected from the ongoing heterozygous breeding at the laboratory so that enough mutant mice are available at P7. The genotyping of mice was performed using the standard polymerase chain reaction (PCR) protocol. The aim is to have a longitudinal follow-up and to show whether the morphological changes at the neonatal age persist and if they worsen with the development of epileptic seizures. Because, these mice breed poorly and many of them do not survive into adulthood, this aim was dependent on the breeding success and survival of mutant mice. P7 mice will be sacrificed, and brains will be fixed by immersion in 4% formaldehyde solution. For cryostat sections, brains will be additionally kept in 20% sucrose solution for two days and frozen by submersion in 2-methyl-butane at -80^{o}C. Brain sections

were cut on a cryostat (frozen sections, 20-µm-thick) from Leica. For the imaging of immunofluorescent staining, the state-of-the-art Zeiss confocal laser scanning microscope LSM 880 and performed the quantitative stereological analysis on an Axio Imager A2 Zeiss fluorescent microscope equipped with the latest Stereo investigator software (Microbrightfield) were used.

Materials and Methods

Materials

- **Substances and buffers**

Table 1 | Substances

Bovine serum albumin	PAA
DAPI Fluormount-G	Southern Biotech
dNTPS	PANBiotech
Fluoromount	Southern Biotech
Ketamine	Albrecht
Lysis buffer (genotyping)	Peqlab
Normal goat serum	Vector
Taq polymerase	Applied Biosystems
Tris pH 7.4	AppliChem
Triton X 100	USBiological
Tween20	AppliChem
Xylazine	Eurovet
PAN ladder 1 (DNA marker)	PANBiotech
OCT	Sakura
Roti ®-Histofix	Carl Roth
Hydrogen peroxide (H2O2)	Sigma Aldrich Chemie
Cannulae, Sterican®	Braun Melsung AG
Microscope cover glasses	Carl Roth GmbH & Co
Microscope object slides	Thermo Scientific
Microtube 1.5 ml	Sarstedt AG & Co
Microtube 15 ml	Sarstedt AG & Co

Pipette tips	Sarstedt AG & Co
Razor blade	Croma

Table 2 | Buffers

Phosphate-buffered saline (PBS)	3 M NaCl 161 mM Na_2HPO_4 x 2 H2O 39 mM KH_2PO_4
Lysis buffer (genotyping)	0.4 mg/ml proteinase K in lysis buffer
PCR buffer (10x)	0.2 M Tris pH 7.9 0.5 M KCl

Table 3 | Primary antibodies

Antigen	Species	Producer	Product Nr.	Dilution in PBS
c-Fos	Polyclonal, Rabbit	Calbiochem	PC05	1:1000

Table 4 | Secondary antibodies

Antigen	Species	Producer	Product Nr.	Dilution in PBS
Rabbit	A546	Goat	Molecular Probes	1:200
Mouse	A546	Goat	Molecular Probes	1:200
Rabbit	Biotinylated Ig	Goat	Vector	1:200

Table 5 | Nucleotide sequences of oligonucleotides used for PCR and expected product size

***SCN2A* gen25**	5'- CCA AAC CAT GAT GGG GGT TAG-3'
***SCN2A* Mut rev**	5'- GAG CTG CAG CCC TAT TAA TAC-3'
***SCN2A* gen30**	5'- GAT CAT GCA CGT TGA AAT GGC-3'
***SCN2A* WTS**	5'- TGT CTG AGT GTC TTT GCT CTC-3'

Table 6 | Products

WT: 391 bp	*SCN2A* gen30 / WTS
Mut: 466 bp	*SCN2A* gen25 / Mut rev

- **Animals and husbandry**

All experimental procedures were approved by the „Landesamt für Natur, Umwelt und Verbraucherschutz Nordrhein Westfalen“, Germany. Animals (mice, Mus musculus) were kept in type II-long plastic cages under standard housing conditions (21 ± 2 °C, 50-70 % relative humidity, and food and water ad libitum, nesting material and a card box houses as well as wood for chewing were provided in the Cologne facilities). Mice were kept on an inverted 12:12 light: dark cycle and fed with Altromin 1314P food (Altromin Spezialfutter GmbH, Lage, Germany). All tests were performed during the dark cycle between 8:30 am and 6:00 pm.

Methods

- **Mouse line generation**

In order to investigate the role of the Nav1.2 channel in human genetic epilepsy, and to characterize functions of Nav1.2 mutation in mice, the human gain-of-function *SCN2A* mutation (p.A263V) was inserted into the *Scn2a* gene locus, and a genetic Nav1.2 channelopathy mouse model was created[67].

To create the knock-in *SCN2A* (A263V) allele, a construct with c.788C>T point mutation flanked by the genomic sequences of *SCN2A* was electroporated into (129/Sv) ES cells. A self-excision cassette was built in vector pKo Scrambler for the selection by neomycin (neo) resistance and excision of the neo resistance gene in the germline. Homologous recombination was confirmed using polymerase chain reaction (PCR). Using the backcross method of the *Scn2a* $^{A263V/+}$ knock-in heterozygotes mouse with C57BL/6J wild-type mice (The Jackson Laboratory), the *Scn2a* $^{A263V/+}$ mutant line was propagated, and the genotypes were verified using polymerase chain reaction. To amplify the mutant *SCN2A* 391-bp fragment*,* 5′-CCAAACCATGATGGGGGTTAG-3′ and 5′-GAGCTGCAGCCCTATTAATAC-3′ primers were used, whereas 5′-TGTCTGAGTGTCTTTGCTCTC-3′ and 5′-GATCATGCACGTTGAAATGGC-3′ primers were used to amplify the wild-type *SCN2A* 466-bp genomic fragment. Mice were kept under standard housing conditions[64].

- **Genotyping**

Isolation of genomic DNA from tail biopsies

Tail biopsies were lysed overnight at 54°C by constant shaking in 75 µl DirectPCR-Tail lysis reagent (Viagen Biotech) containing 0.2 mg/ml Proteinase K. Then, lysed tail biopsies were incubated for 45 min at 85°C to inactivate Proteinase K.

Isolation of genomic DNA from ear biopsies

Ear biopsies were lysed overnight at 54°C under constant shaking in 75 µl lysis buffer (100 mM NaCl, 50 mM Tris HCl pH 8.0, 1 mM EDTA, 0.2% Nonidet P-40, 0.2% Tween 20, 0.1 mg/ml Proteinase K).

Polymerase chain reaction

Polymerase chain reaction (PCR) was performed to detect *SCN2A* (A263V) mutation. Reactions were performed in a thermoblock (T3 Thermocycler, Biometra®) with a reaction volume of 50 µl. Program applied is given in Table 7.

Table 7 │Protocol (50µl)

***SCN2A* gen25 (50 pmol)**	0.6 µl
***SCN2A* gen30 (50 pmol)**	0.6 µl
***SCN2A* WTS (50 pmol)**	0.4 µl
***SCN2A* Mut rev (50 pmol)**	0.4 µl
10 x PCR-Buffer	5.0 µl
dNTPs	0,5 µl
Dream Taq	0.2 µl
H_2O	40.3 µl
DNA template	2.0 µl

Cycle	Step description	Temperature	Duration
1	initial denaturation	95°C	3 min
	denaturation	95°C	30 s
2-7	annealing	60°C- 1°C/cycle	30 s
	elongation	72°C	45 s
	denaturation	95°C	30 s
8-38	annealing	55°C	30 s
	elongation	72°C	45 s
39	final elongation	72°C	5 min

Hybridization temperatures were gradually lowered by 1°C per cycle.

Agarose gel electrophoresis

After PCR reaction, 10 µl of 5x loading dye (50% glycerine, 60 mM EDTA, 0.025% xylene cyanol, 0.025% bromophenol blue) was added to 50 µl PCR product, and 18 µl PCR product containing loading dye was loaded into agarose gel wells (2 % agarose in 1x TAE buffer (40 mM Tris, 10 mM acetic acid, 1 mM EDTA pH 8.0) and electrophoretically separated in 1x TAE buffer at 130V.

- **Histology**

Tissue preparation

For the histological analysis of the brain at the age of P7, animals were sacrificed by cardiac perfusion. Here mice were weighed and anesthetized with intraperitoneal (i.p.) injections of ketamine (100 mg/ml) and xylazine (20 mg/ml) in 0.9% NaCl solution. After sufficient anesthesia and analgesia had been achieved, the thorax was carefully opened, and the heart was exposed. At room temperature (RT), 4 % PFA (Roti® Histofix, Roth) was perfused by a 25-gauge cannula through the left ventricle to remove blood from the body of the mouse and to fixate the tissue. Approximately 50 ml solution was used per animal. Following perfusion, the brains were left in situ for approximately 2 hours at RT to reduce fixation artifacts. Mice were then decapitated, and the brain was carefully removed and immersed in 4 % PFA overnight at 4°C.

For cryoprotection, the tissue was then moved to 20 % sucrose in phosphate- buffered saline (PBS) pH 7.3, at 4°C for two days.

All brains were promptly frozen by insertion into 2-methyl-butane (isopentane), which had been precooled to -80 °C on dry ice. Frozen brains were stored at -80 °C until further treatment.

Preparation of tissue for sectioning

For sectioning, the caudal pole of each brain was attached to a cryostat specimen holder using a pre-frozen layer of Tissue Tek (Sakura Finetek Europe, Zoeterwoude, Netherlands). The ventral surface of the brain was oriented to face the cryostat knife edge, and serial coronal sections were cut in a cryostat Leica CM3050 (Leica Instruments, Nußloch, Germany) in 20-µm-thick sections and mounted on SUPERFROST® PLUS (Thermo scientific) microscope slides. Since stereological analyses require extensive sectioning of the structures studied and the use of spaced-serial sections[76], sampling was always done in a standard sequence. In the

end, 4 sections that were 400µm apart from each other were present on each slide (Figure 5) and stored at -20 °C until staining.

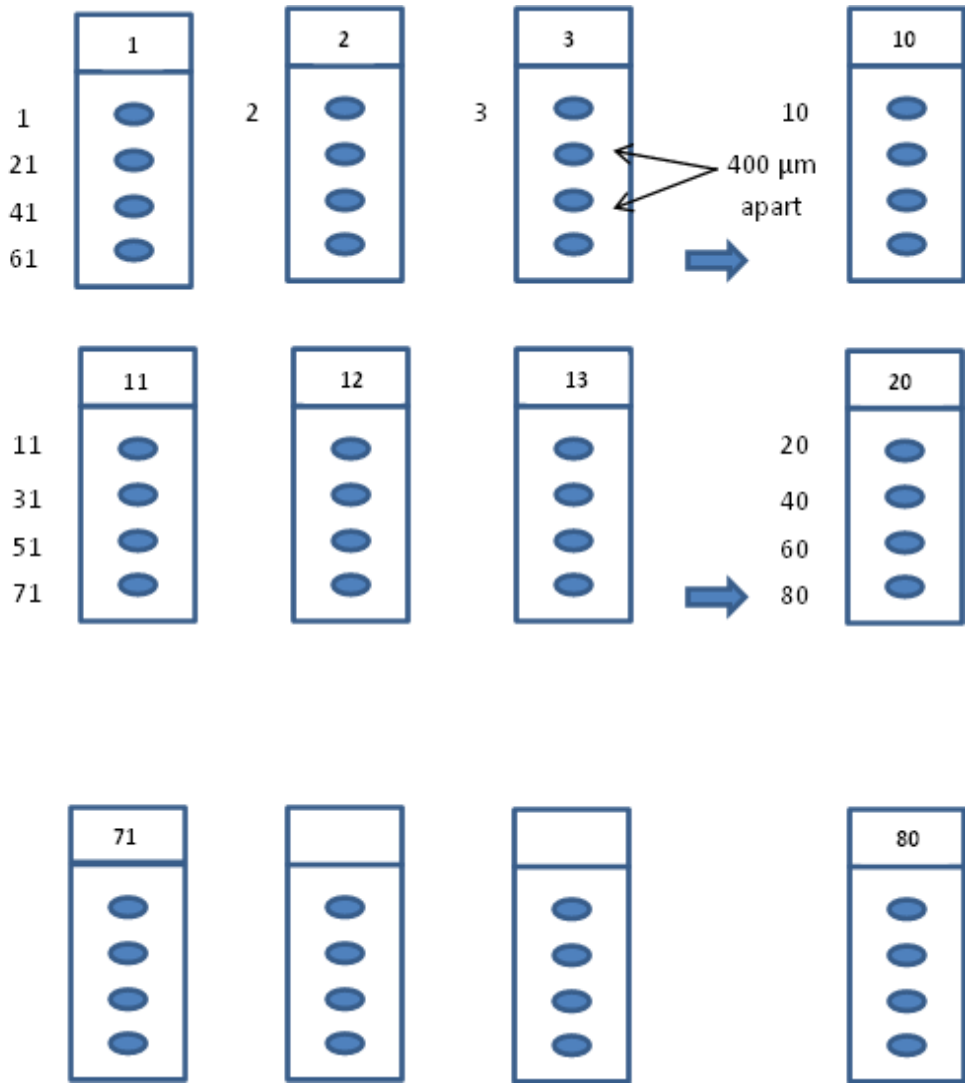

Figure 5| ***Standardized sequence of collecting sections (20µm) on glass slides.*** Staining of slides from one row (e.g., 1, 11, etc.) with a given antibody (see below) provides the opportunity to evaluate a cell population using randomly spaced samples from a brain structure of interest.

Immunohistochemistry

For immunohistochemistry, different protocols were applied to yield the best possible staining.

Staining of c-*Fos* as a marker of neuronal activity

Sections were shortly washed in PBS to remove the Tissue-Tek. For detection of c-Fos antigens, the avidin-biotin-complex (ABC) method was used. The ABC method takes advantage of the high affinity between biotin and the four biotin-binding sites of avidin, allowing the establishment of a connection between a pre-formed avidin-biotin-peroxidase complex and the antigen-antibody complex. In the presence of H_2O_2, the peroxidase oxidizes the chromogene 3, 3´-diaminobenzidine (DAB) to a precipitating dye.

Sections were washed with PBS, incubated in 0.3% H_2O_2 solution for 30 min to inhibit endogenous peroxidases, and washed 3 times for 15 min. Unspecific binding of the antibodies was reduced by blocking with 5 % normal goat serum and 0.2 % TritonX-100 in PBS for 1 hour at room temperature. The primary antibody was diluted in PBS 1:1000 and 250 µl/slide were incubated overnight at 4 °C in a humid chamber. Thereafter, the slides were washed three times for 15 min in PBS on a shaker. Anti-rabbit secondary antibody diluted 1:200 in PBS was applied for 2 hours at room temperature in a humid chamber in the dark and washed with PBS three times for 15 min on a shaker. Sections were incubated for 2 h with the preformed avidin-biotin complex using VECTASTAINR ABC-Elite Kit (Vector laboratories) prepared according to manufacturer's instructions, washed 4 times for 5 min in PBS, and subsequently incubated in DAB substrate solution (SIGMA FAST™ 3,3´-Diaminobenzidine tablets, Sigma) until staining became visible. To stop the reaction, slices were carefully washed 4 times in water. Slices were then mounted on SUPERFROST® PLUS microscope slides and dehydrated in an ethanol series (70%, 90%, 98%, twice 100% ethanol and twice RotiR Histol (Roth)) and cover slipped with RotiR Histokitt.

Nissl staining

For visualization of brain morphology and cell bodies of neurons, respectively, the basic dye cresyl violet was used. The dye labels the negatively charged ribonucleic acid (RNA) of the rough endoplasmatic reticulum. Slices were mounted on SUPERFROST® PLUS (Thermo Fisher Scientific) microscope slides and tried at 37°C for 1 h. They were then incubated in cresyl violet solution (9 g/l cresyl violet, 10% ethanol) for 3 min. Excess stain was removed using 1% acetic acid in 96% ethanol and, subsequently, slices were rinsed in 96% ethanol followed by two rinsing steps in 99.9% ethanol. This was followed by two steps of incubation in xylol for 5 min and slices were cover-slipped with RotiR Histokitt II (Roth).

Microscopy

Brain sections were investigated with a Zeiss AX10 microscope using AxioCam MRc or AxioCam MRm cameras using the Zen 2 lite software.

Stereological analysis

Brains were analyzed blind to the experimental conditions and hemispheres. Stereological analyses were performed with the Stereo Investigator Software Version 10.01 from MicroBrightField at an AxioImager microscope. For c-*Fos* the optical dissector method was chosen for quantitative analysis because of its efficiency[76], an important prerequisite for the quantification of numerical densities of a variety of cell types in a given brain region [79].The method consists of direct counting of objects in relatively thick sections under the microscope using a three-dimensional counting frame ("counting brick" of Howard and Reed, here simply referred to as dissector) to "probe" the tissue at random. The area viewed was randomized by setting a reference point at an arbitrary place, resulting in an overlay of the visible field by a grid. Sections cut at distances between 3 and 4mm caudally to the rostral pole of the forebrain (where the collection of the sections began) were observed under low-power magnification (10 x objectives) to subdivide the hippocampus. The areas of the whole hippocampal region, of the pyramidal cell layer CA1, CA3, and of the granular cell layer in the dentate gyrus were encountered separately by measuring frame. The area of the entorhinal cortex was divided into superficial layers L1-L3 and deep layers L4-L6.

The base of the frame (dimensions in the x/y plane) is defined by the size of the squares formed by a grid projected into the visual field of the microscope. The height of the dissector is a portion of the section thickness defined by two focus planes in the z axis at a distance of x µm. Control of this parameter is achieved by the use of mechanic or electronic devices measuring the movement of the microscope stage in the z axis. As an exception to the stereological counting rules, objects (stained nucleus of the neurons) within each dissector squares within the marked area, at distances of 100 µm with a dissector depth of 12 µm, were labelled with different symbols for each counting frame, starting from the uppermost left side of the field and including those being entirely within the dissector and those touching or being dissected by the "acceptance", but not the "forbidden", planes of the frame are counted by using the 20x magnification objective. All marked frames were consecutively viewed. Three sections were evaluated per animal and staining.

Statistics

Unless otherwise stated, group measures are given as mean ± standard error of the mean (S.E.M.) Statistical analysis was performed using the software STATISTICA (StatSoft, Tulsa, Oklahoma) and GraphPad Prism (GraphPad Software, Inc., La Jolla, California). Mutant mice and their respective littermate controls were compared with a student's t test or Mann-Whitney U test when data did not meet the requirements for parametric analysis. Prior to statistical test data were tested for normality of distribution, using Shapiro-Wilk test and the Equal Variance test. Only if both tests were passed, parametric t test was applied. In all cases where either normality and/or equal distribution test failed, non-parametric Mann-Whitney test was used. To compare values to expected chance, either a parametric one-sample t test or a nonparametric Wilcoxon signed-rank test was applied. All tests were unpaired, two-tailed and significance was accepted at $p < 0.05$. Additionally, we performed a two-way analysis of variance (ANOVA) with independent factors "genotype" and "treatment" for each subregion separately.

Animal identification system

For identifying the neonatal mice, a tattoo is placed on a toe by the age of P0. Disinfection of mice skin and the tattoo needles was applied before tattooing a mouse.

Phenytoin preparation for subcutaneous injections and B-cyclodextrin

To prevent the tissue damage caused by subcutaneous or intramuscular administration of phenytoin[80] we dissolved it in a beta-cyclodextrin medium as follows:

We transferred 10 ml PBS from the sterile bottle under the cell culture hood into 50 ml tube, then we dissolve 2.1g beta-cyclodextrin in it for a 21% solution. We Adjusted the Solution pH with target 8.0 by adding a total of 90 µl 0.1N NaOH. The we dissolved a 600 µl of phenytoin in the 10 ml CD (in PBS) with continuously adjusting the pH of the solution to 8.0.

B-Cyclodextrin is an oligosaccharide consisting of seven glucose subunits joined by α-(1,4) glycosidic bonds used as a dissolving agent in drug preparation. It forms with a poorly water-soluble drug molecule an inclusion complex which increases its aqueous solubility[81].

Plasma level of phenytoin and dosage

to monitor our therapy and to exclude an accumulation of the drug I measured the total phenytoin plasma level in a pooled blood sample of 5 neonatal mice at the age of P7 after treatment with 10 ug/g phenytoin every 12 hours twice a day for 7 days. The drug was injected

subcutaneously on the back side of neck using Hamilton chromatography syringe. The phenytoin measurements were done by the Dept. of Clinical Chemistry of the University Hospital Cologne (Dr. Streichert).

Results

Measurement of total phenytoin plasma concentrations

It has been measured the total phenytoin plasma level in a pooled blood sample of 5 neonatal mice at the age of P7 after treatment with 10 ug/g phenytoin every 12 hours twice a day for 7 days.

It shows a concentration of 11 mg/l (reference range 10-20 mg/l) which proved that our dosage was in the target range and would exclude an accumulation of the drugs in the mice tissues.

Neuronal network activity in the hippocampus region after treatment with phenytoin for 7 days as compared to the littermates treated with B-cyclodextrin as a control group

As our mouse line SCN2A (p.Ala263Val) has a gain-of-function mutation of the sodium channels, which should respond to a treatment with sodium channel blockers (SCBs), it has been planned to treat the mice with phenytoin starting at the age of P0 for initially 7 days, as the first checkpoint of the study and for 14 days in the second phase.

In 7-day-old mice, the number of neurons expressing nuclear c-FOS immunoreactivity in each structure of the hippocampus (CA1, CA3, and DG) was significantly lower in phenytoin treated Scn2a (A263V) mice, as compared to their littermates treated with cyclodextrin in all Scn2a (A263V) groups (homozygous mutant, heterozygous mutant and wild-type mice) (Figure 6, 7, 8 and 9). We first analyzed, subregion specific, differences between phenytoin treated mice and cyclodextrin controls (Figure 6, 7, and 8). In the CA1 subregion, phenytoin treated mice showed fewer c-FOS immunoreactive cells in wild-type (Mann Whitney, $U = 0$; $p = 0.037$), heterozygous mutant (Mann Whitney, $U = 0$; $p = 0.036$) and homozygous mutant mice (t test, $t(6) = 6{,}036$; $p < 0.001$) (Figure 6). In the CA2-3 subregion, phenytoin treated mice showed fewer c-FOS immunoreactive cells in wild-type (t test, $t(6) = 6{,}247$; $p < 0.001$), heterozygous mutant (t test, $t(6) = 7.317$; $p < 0.001$) and homozygous mutant mice (t test, $t(6) = 10.174$; $p < 0.001$) (Figure 7). Finally, for DG subregions the results were similar for wildtype (Mann Whitney, $U = 0$; $p = 0.037$), heterozygous mutant (Mann Whitney, $U = 0$; $p = 0.036$) and homozygous mutant mice (Mann Whitney, $U = 0$; $p = 0.036$) (Figure 8). We also compared the differences between various treatments (no treatment, phenytoin treatment and cyclodextrin control) in different subregions, as shown in figure 9. The comparison was performed using a two-way analysis of variance (ANOVA) with independent factors “genotype” and “treatment”, again for each subregion separately.

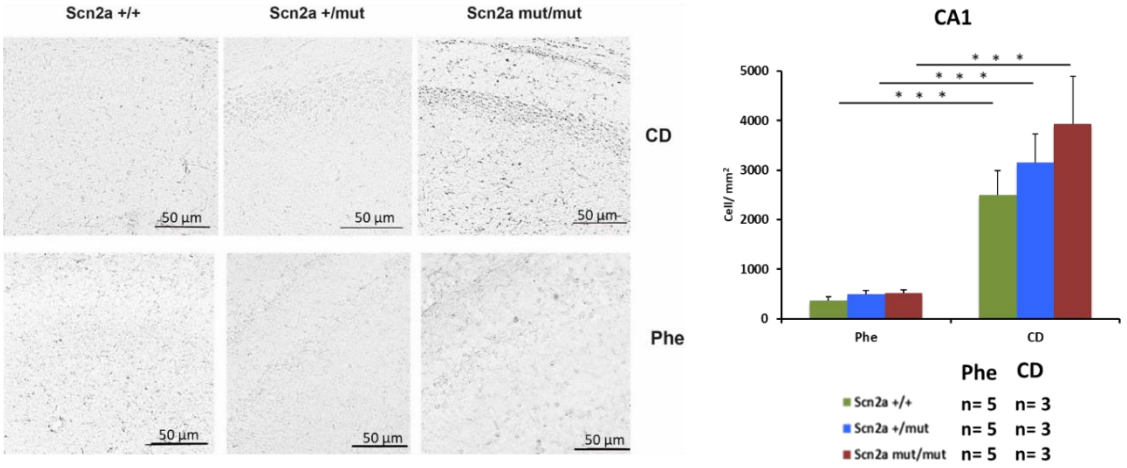

Figure 6| ***c-FOS immunoreactivity in hippocampal regions*.** Number of neurons stained for c-FOS in the CA1 subregion of the hippocampus of P7 Scn2a homozygous mutant (n=5) mice, their wild-type (n=5) and heterozygous mutant littermates (n=5) after treatment with phenytoin for 7 days in comparison to their littermates P7 Scn2a homozygous mutant (n=3) mice, their wild-type (n=3) and heterozygous mutant littermates (n=3) which were treated with B-cyclodextrin. Results are presented as mean values + S.E.M. of profile density (number of cells/mm^2), *p<0.05; **p<0.01, ***p<0.005; two-tailed t test.

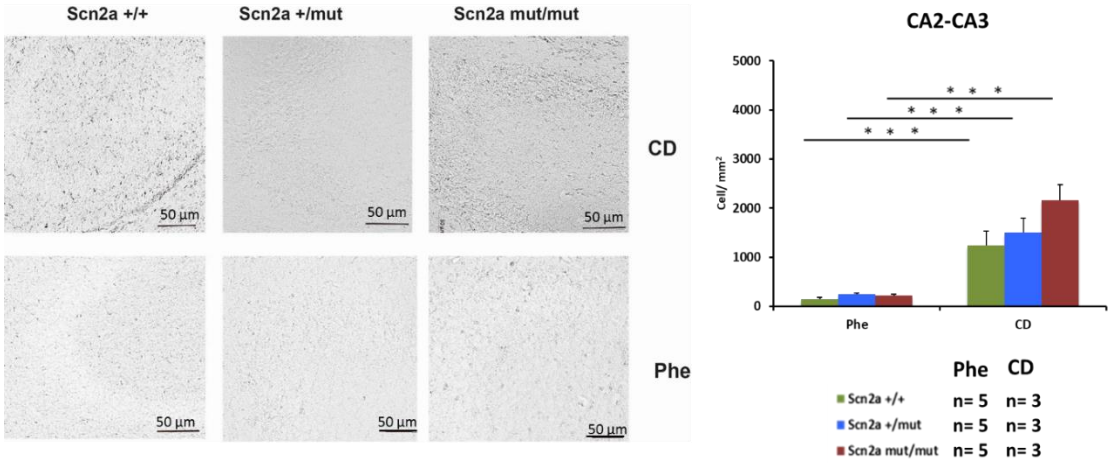

Figure 7| ***c-FOS immunoreactivity in hippocampal regions*.** Number of neurons stained for c-FOS in the CA2-CA3 subregion of the hippocampus of P7 *Scn2a* homozygous mutant (n=5) mice, their wild-type (n=5) and heterozygous mutant littermates (n=5) after treatment with phenytoin for 7 days in comparison to their littermates P7 *Scn2a* homozygous mutant (n=3) mice, their wild-type (n=3) and heterozygous mutant littermates (n=3) which were treated with B-cyclodextrin. Results are presented as mean values + S.E.M. of profile density (number of cells/mm^2), *p<0.05; **p<0.01, ***p<0.005; two-tailed t test.

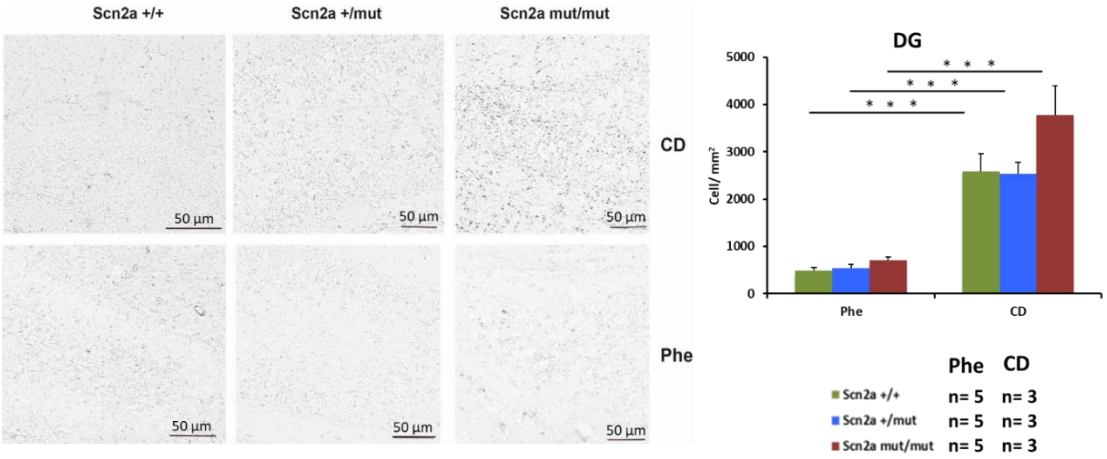

Figure 8| ***c-FOS immunoreactivity in hippocampal regions***. Number of neurons stained for c-FOS in the DG subregion of the hippocampus of P7 *Scn2a* homozygous mutant (n=5) mice, their wild-type (n=5) and heterozygous mutant littermates (n=5) after treatment with phenytoin for 7 days in comparison to their littermates P7 *Scn2a* homozygous mutant (n=3) mice, their wild-type (n=3) and heterozygous mutant littermates (n=3) which were treated with B-cyclodextrin. Results are presented as mean values + S.E.M. of profile density (number of cells/mm^2), *p<0.05; **p<0.01, ***p<0.005; two-tailed t test.

Interestingly, in 7-day-old mice, the number of neurons expressing nuclear c-FOS in each structure of the hippocampus (CA1, CA3, and DG) was significantly higher in cyclodextrin (vehicle)-treated *Scn2a* (A263V) mice, as compared to their not-treated littermates in all *Scn2a* (A263V) groups (homozygous mutant, heterozygous mutant and even though wild-type mice) (Figure 9). When two-way ANOVA was applied, to analyze the effect of genotype and treatment on the number of c-FOS-expressing neurons. For the CA1 simple main effects analysis showed that genotype did not have a statistically significant effect on the number of c-FOS expressing neurons (p = 0,051), but treatment had (P < 0,001). For the CA3, both genotype (p = 0.002) and treatment (P < 0,001) had significant effects, as well as for the DG (genotype p = 0.001; treatment p < 0.001), These results, however, have to be taken with caution, as the significant interaction between genotype and treatment was present in all 3 regions (p = 0.007, p = 0.001, p = 0.002 for the CA1, CA3 and DG, respectively). We also performed pairwise multiple comparisons according to the Holm-Sidak method. For the CA1, In all three genotypes, phenytoin treatment caused a significant difference in the number of c-FOS positive neurons (p < 0.001), as was the case for the CA3 (p < 0.001) and the DG (p < 0.001).

The number of neurons expressing nuclear c-FOS in each structure of the hippocampus (CA1, CA3, and DG) shows no significant difference in phenytoin-treated *Scn2a* (A263V) mice as compared to their not-treated wild-type littermates *Scn2a* (A263V) group (Figure 9; $p < 0.001$)

Unfortunately, none of the 14 days phenytoin-treated homozygous mutants survived to be analyzed as initially planned for the second phase of my study.

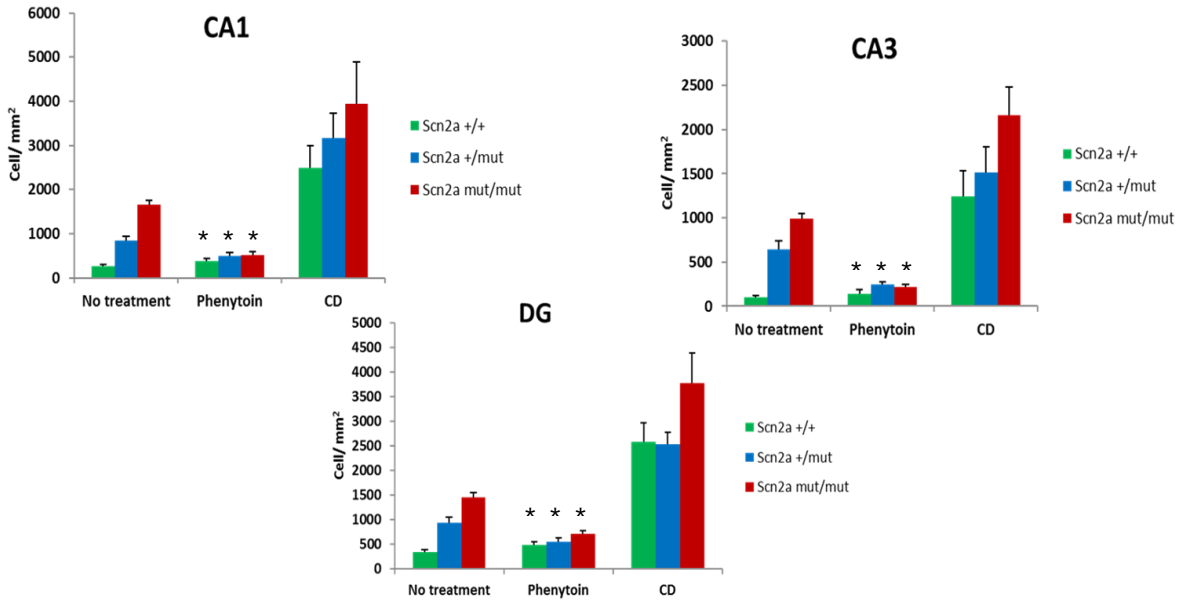

Figure 9| ***A comparison of the c-FOS immunoreactivity in the hippocampal regions among non-treated, treated with phenytoin and treated with B-cyclodextrin 7 days old mice***. Number of neurons stained for c-FOS in the CA1, CA2-CA3, and DG subregion of the hippocampus of P7 Scn2a before and after treatment with phenytoin for 7 days in comparison to their littermates which were treated with B-cyclodextrin. Results are presented as mean values + S.E.M. of profile density (number of cells/mm^2), *p< 0.001, two-way ANOVA with Holm Sidak post-hoc test.

C-Fos immunoreactivity as a reflection of neuronal network activity in the entorhinal cortex of 7-day-old *Scn2a* (A263V) mice

To investigate number of neurons expressing nuclear c-FOS immunoreactivity in the entorhinal cortex, I divided the entorhinal cortex depending on its connectivity network to the hippocampus into deep layers (L4-L6) and superficial layers (L1-L3) (Figure 10)

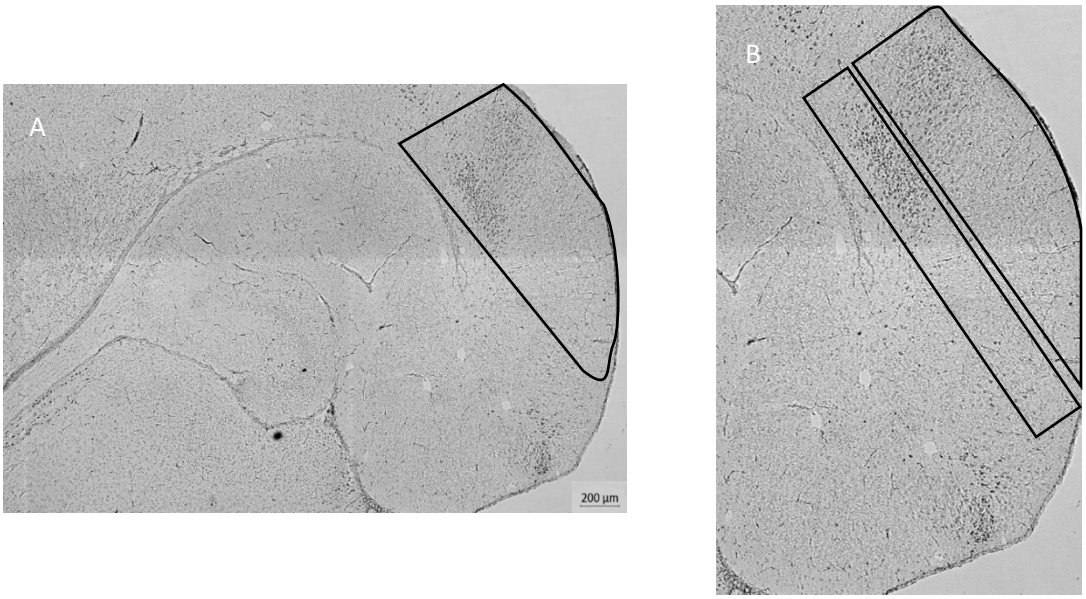

Figure 10│ **c-*FOS immunoreactivity in the entorhinal cortex.*** (A) Representative low-power view image of c-FOS immunostaining in *Scn2a* wild-type (A; *Scn2a* +/+) mouse. (B) Higher magnification image medial and dorsal entorhinal cortex in a horizontal section divided in the superficial L1-L3 and deep layers L4-L6. Scale bars: 200 µm (A) and 50 µm (D).

In 7-day-old mice, the number of neurons expressing nuclear c-FOS immunoreactivity in deep layers of the entorhinal cortex (L4-L6) was significantly higher in homozygous (t test, t(4) = 2,163; p = 0.097) and heterozygous (Mann Whitney, U = 0; p = 0.016) Scn2a (A263V) mutant mice as compared to superficial layers (L1-L3) (Figure 11).Similarly, a significant difference in the number of neurons expressing nuclear c-FOS immunoreactivity in deep layers of the entorhinal cortex (L4-L6) in homozygous as compared to the heterozygous (t(6) = 3.5; *Scn2a* (A263V) mutant mice.

On the other hand, there was no significant difference between the deep and superficial layers of the entorhinal cortex in the number of neurons expressing nuclear c-FOS immunoreactivity in wild-type littermates, Mann-Whitney rank sum test, U = 6, p = 0.686 (Figure 11). We can conclude that deep layers of the entorhinal cortex may play an important role in seizure activity in the A263V mutant mice by the propagation of hippocampal hyperactivation to cortical regions.

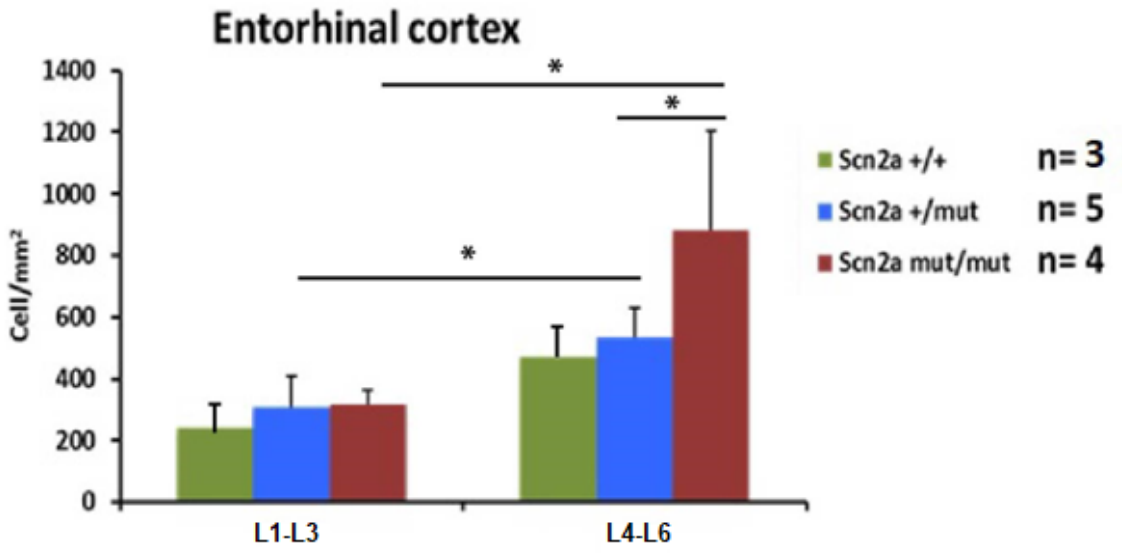

Figure 11 **| *Neuronal network activity in the entorhinal cortex layers.*** Number of neurons stained for c-FOS in the deep entorhinal cortex layers L4-L6 and superficial layers L1-L2 of P7 *Scn2a* homozygous mutant (n=4) mice, their wild-type (n=3) and heterozygous mutant littermates (n=5). Results are presented as mean values + S.E.M. of profile density (number of cells/mm^2), *p<0.05; **p<0.01, ***p<0.005; two-tailed t test

Discussion

My previous work on the Nav1.2 epilepsy mouse model showed that the neuronal network hyperactivity in the hippocampal region in 7-day-old mice is the likely area of origin of the seizures[72], and by considering the well-known Hippocampus- Entorhinal Cortex Connectivity; an important question emerged, is the Nav1.2 mutation led to network hyperactivity in the Entorhinal Cortex and if does, where is the hyperactivity began from.

In this study, I aimed first to answer these questions by investigating a potential layer-specific neuronal activation in the entorhinal cortex.

After that, I investigated the effect of the phenytoin treatment during the neonatal period on the extent of neuronal activation in the hippocampus of 7-day-old mice measured by the quantification of c-Fos immunoreactivity.

Activation of the hippocampal neuronal circuit

The entorhinal cortex (EC) is a well-known important connection point between the hippocampal formation and other cortical areas, and its name came from the fact that it is enclosed by the rhinal sulcus in the human brain[91].

Subdivision of cortical areas defined by their connection schemes is more reliable to understand their role in a variety of brain diseases[92]. Therefore, subdividing the EC based on its hippocampal connectivity, as initially proposed by Ramón Y Cajal, is the most consistent concept. The input from the entorhinal cortex layers II and III is the main projection to the hippocampus. Neurons in layer II give the entorhinal projections to the dentate gyrus, CA2 and CA3 fields, whereas neurons in layer III form the core projections to CA1 and subiculum. On the other hand, the hippocampal fields CA1 and subiculum are the main input to layer V of the EC, which in turn the central EC output to cortical and subcortical areas in the forebrain [91].

The entorhinal cortex in rodents can be divided based on its hippocampus connectivity in lateral EC (LEC) and medial EC (MEC)[60]. **The medial EC** is characterized by a consistent six-layered arrangement and a regular distribution of neurons in all layers. In layer II there are two main neurons, excitatory pyramidal medium-sized neurons and large multipolar ones known as the stellate cells (SCs). The laminar arrangement in **the lateral EC** is less consistent and the distribution of neurons in all layers is less regular. In layer II in compared to the medial EC

there are three main neurons, excitatory pyramidal and multipolar medium-sized neurons and large multipolar ones known as fan cells[91].

The layer V principles cells can be divided into two sublayers Va, which is nearby layer IV (lamina dissecans), with its large pyramidal unevenly scattered neurons projecting to different cortical and subcortical areas. On the other hand, sublayer Vb, adjacent to layer VI with its smaller dense and regular distributed neurons which integrate the input originating from the neurons of CA1, subiculum as well as layer II of EC, which make sublayer Vb a main structure of the intrinsic deep to superficial circuit[91,93].

Another cell population of the sublayer Vb are GABA-negative/calretinin-positive neurons[91,94]

Entorhinal cortex Networks

Extrinsic Networks

The superficial layers of the entorhinal cortex, mainly layer I, receive significant projections from olfactory areas[95,96], whereas layer II receives projections from the orbitofrontal area, postrhinal cortex and pre- and parasubiculum. Additionally, layer V receives input from infralimbic, prelimbic cortex, pre- and parasubiculum[91,97–99].

Intrinsic Networks

- **Layer II**

Neurons in EC can be divided in calbindin- and reelin-expressing cells, which are patch-like organized in the MEC and separately distributed in sublayers in the LEC; reelin-expressing in layer IIa and calbindin-expressing cells in layer Iib[91].

Reelin-expressing neurons make mainly connections with dentate gyrus and CA3, whereas calbindin- expressing neurons make connections with CA1 and the contralateral EC[100].

Interestingly, neurons in layer III of the EC also make important functional connections with the contralateral hippocampus and EC[101].

The SCN2A gain-of-function (p.Ala263Val) mutation disturbs a highly conserved amino acid in Nav1.2 and leads to neonatal onset of neuronal hyperexcitability by slowing the inactivation time course due to a depolarizing shift in which more channels are available for activation at resting membrane potential, and on the other hand, increasing the persistent sodium current

which in turn causes a depolarization of neurons membrane leading to synaptic potentials amplification and subthreshold oscillations generation.

It has been proposed that neurons in layers II and III deliver different input combinations to the hippocampal formation and a copy of that information to neurons in layer V. On the other hand, neurons in layer V receive a copy of the information processed by the hippocampus through their connection with CA1 and the subiculum. By taking into account the EC intrinsic connectivity between layer V and layers II and III, it is hypothesized that a copy of the processed information in layer V will be delivered back to the superficial layers, which make these neurons in layer V of EC an important integrating point in the input processing and the hippocampal-cortex connectivity[91].

It was reported by[103] depending on their EEG study on freely acting cats that medial EC is connected to the hippocampus and lateral EC is connected to olfactory areas.

In another study it has been shown that input from olfactory areas is followed by neuronal activation in MEC, LEC and hippocampus[104].

The hippocampus drives the epileptogenesis and the entorhinal cortex propagates it

Interestingly, my results confirmed the assumption that the Nav1.2 mutation could lead to network hyperactivity not only in the hippocampus but also in the Entorhinal Cortex, and it also showed a significant difference in the number of neurons expressing nuclear c-FOS immunoreactivity in the deep layers of the entorhinal cortex (L4-L6) as compared to the superficial layers (L1-L3) in homozygous and heterozygous Scn2a (A263V) mutant mice in a gene dose-dependent manner.

These findings of layer and gene dose-dependent neuronal activation differences in between the entorhinal cortex could be well explained by an increased output of the hippocampus to the entorhinal cortex, which in turn led us to conclude that the hippocampus, as hypothesized, drives the epileptogenesis and the entorhinal cortex propagates it.

Treatment options and time window in the first two weeks

It was critical for the therapy planning of Nav1.2 mutation-induced epilepsy to take into consideration the kinetics of the drug on sodium channels subtypes which possess a high level of conservation (phenotypic spectrum and genetics of SCN2A-related disorders, treatment options, and outcomes in epilepsy and beyond).

Depending on my findings of higher neuronal activation in the hippocampus of 7-day-old *Scn2a* (A263V) mice and the fact that SCN2A subunits are highly expressed during the first two weeks of life high in the hippocampus and cortex[34,84], the treatment of SCN2A gain-of-function diseases should likely start already at birth.

I focused mainly on my therapeutic strategy of using an antiepileptic drug that can inhibit the incidence of the first seizure and prevent the epileptogenic changes caused by neuronal circuit reorganization and increasing of the seizure threshold to possibly inhibit epileptogenesis[85].

Of note, since rodents are born more immature than humans, the first two neonatal weeks in mice correspond approximately to the last trimester of human pregnancy[107].

Treatment and outcome

It has been reported that infantile or early childhood onset SCN2A-induced seizures are drug-resistant in up to 100% and that the most efficient drug in this group of patients was phenytoin with around 50% of seizure reduction. Unfortunately, to achieve this seizure reduction high doses of phenytoin were needed, which implicated a therapeutic difficulty by increasing the side effects and inducing a difficult interaction profile since phenytoin has nonlinear elimination kinetics. On the other hand, it was reported that phenytoin was not effective, or even worsened the seizures in some gain of function and in late-onset SCN2A-related epilepsies[44,105].

Since my experiment goal was to understand the effect of phenytoin on the C-Fos expression as an indirect marker of seizure frequency of the seven-day-old pups, it was important to minimize external stimulation during the experiment. Therefore, the mice were brought back to their nest after each injection without implanting an electrode to detect epileptic seizures, which, at this age, would have been a terminal experiment. Therefore, I could not assess the frequency of seizures before and after the treatment with phenytoin. A different experimental approach that enables the detection of seizures is therefore needed to monitor the treatment effect.

Suppression of neuronal hyperexcitability driven by *Scn2a* mutation after 7 days of treatment with phenytoin

As I found in my previous work[109] that the p.A263V mutation in Nav1.2 led to neuronal network hyperactivity in the hippocampal region by quantifying the nuclear immunohistochemical staining for the c-FOS transcription factor as well as that continuous electroencephalogram monitoring of *Scn2a* (GAL879-881QQQ) mutant mice showed focal seizure activity in the

hippocampus[18] and the deep electrode EEG recordings from P7 and P14 *Scn2a* (A263V) mutant mice[108] These previous findings support the hypothesis that the seizures caused by a *Scn2a* (A263V) missense mutation are most likely of hippocampal origin.

The significant difference in the c-Fos expression between the *Scn2a* mutant mice after phenytoin treatment and their matched untreated littermates in this study shows a reduction of neuronal hyperexcitability driven by *Scn2a* gene mutation despite the lack of experimental proof of seizure suppression by the age of 7 days.

On the other hand, the significant difference in the c-Fos expression between the *Scn2a* mutant as well as wild-type mice after phenytoin treatment and their matched cyclodextrin/vehicle-treated littermates could certainly be explained by the sodium channel-blocking effect of phenytoin and but also by stress-induced activation during the injection of cyclodextrin. Interestingly, since phenytoin could prevent stress-induced neuronal impairment and atrophy of hippocampal pyramidal neurons[88,89] which could explain the reduced neuronal activity despite the stress stimuli for the pups induced by phenytoin injection.

The maternal stress-induced changes could not be significantly apparent by the age of 7 days, but I will discuss later in this work their long-term effects and the increased mortality of the mutant pups after phenytoin treatment for two weeks.

Comparing the c-Fos expression between the Scn2a wild-type mice after phenytoin treatment and their matched untreated littermates I found no significant difference which implies that phenytoin treatment would not reduce the normal intrinsic neuronal activity but just the epileptiform or the extrinsic induced one. This finding supports the conclusion that phenytoin decreases synaptic transmission and suppresses epileptiform activity without affecting the intrinsic neuronal firing mechanisms[90].

Discussing the significant difference in the c-Fos expression between the Scn2a homozygous mutant mice and their matched heterozygous mutant littermates after cyclodextrin treatment would strengthen the conclusion I found in my previous work that the A263V mutation in Nav1.2 has an important effect on neuronal hyperactivation in a gene dose-dependent manner.

Interpreting these findings led us to conclude that phenytoin had significantly reduced the neuronal hyperactivation triggered by SCN2A mutation which in turn will mean seizure reduction in P7 mice.

Limitations and difficulties

Another interesting finding was that the weight gain of the pups under phenytoin treatment was less than their siblings under cyclodextrin treatment. It could be explained by the side effects of phenytoin on the gastrointestinal tract and liver function. But taking into consideration the seizures and post-seizure time by mutant mice and their correlated sedation, we could explain their reduced weight gain by reduced nursing time for mutant pups and less competition for wild-type ones.

Considering that *SCN2A* mutations are linked to autism and behavioral retardation[18], these processes could reduce or interfere with epileptogenesis therapeutic outcome by affecting the maternal behavior and the dam-pups relationship. The significant differences I found in this study in the c-Fos expression between the *Scn2a* mutant and especially wild-type mice after cyclodextrin treatment and their matched untreated littermates support this theory and suggest that it is important to investigate alternative application forms of the anti-epileptic drugs in neonatal pups. Taking into account the maternal separation stress, the enteral drug application during this neonatal age window was unfortunately not practical and could only be avoided with a slow-release formula or small osmotic pump.

On the other hand, the daily two-time injection process for the neonatal mice was probably stressful since I needed to move them out of their warm nest away from their mother and then performed the subcutaneous injection, which could have induced a seizure in mutant mice with low seizure threshold[86].

This process could also cause a maternal stress activation which in turn could induce nursing and lactation changes either by direct targeting of the maternal and consequently the pup's hypothalamic-pituitary-adrenocortical axis or by inducing maternal behavior changes[87].

Given these caveats, it is currently unclear, to which extent findings from treatments in rodent disease models can be extrapolated to human patients.

Taking into consideration that the projections of the EC to the dentate gyrus are not well preserved as the connection and its projections between the EC and the CA1 area in mammalian species make the extrapolation of these findings from rodents to humans difficult[91].

Conclusion

The main finding of this study strongly supports the hypothesis that the seizures caused by a Scn2a (A263V) missense mutation are most likely of hippocampal origin and entorhinal cortex propagation. Moreover, the results of this study broaden our understanding of how this channelopathy influences the development of a hyperexcitable epileptogenic brain during the neonatal period.

It also showed that Phenytoin despite the difficulties in its application strategy is an effective treatment to suppress seizures and to prevent epileptogenesis in a genetically altered brain development.

References

1 Stafstrom CE, Carmant L. Seizures and epilepsy: an overview for neuroscientists. *Cold Spring Harbor perspectives in medicine* 2015; **5**. DOI:10.1101/cshperspect.a022426.

2 Menezes LFS, Sabiá Júnior EF, Tibery DV, Carneiro L dos A, Schwartz EF. Epilepsy-Related Voltage-Gated Sodium Channelopathies: A Review. Frontiers in Pharmacology. 2020; **11**. DOI:10.3389/fphar.2020.01276.

3 Coorg R, Weisenberg JLZ, Wong M. Clinical neurogenetics: recent advances in the genetics of epilepsy. *Neurologic clinics* 2013; **31**: 891–913.

4 Cascino GD. When drugs and surgery don't work. *Epilepsia* 2008; **49 Suppl 9**: 79–84.

5 Falco-Walter JJ, Scheffer IE, Fisher RS. The new definition and classification of seizures and epilepsy. Epilepsy Research. 2018; **139**. DOI:10.1016/j.eplepsyres.2017.11.015.

6 Devinsky O, Vezzani A, O'Brien TJ, *et al.* Epilepsy. Nature Reviews Disease Primers. 2018; **4**. DOI:10.1038/nrdp.2018.24.

7 Berkovic SF. Genetics of Epilepsy in Clinical Practice. *Epilepsy currents* 2015; **15**: 192–6.

8 Kirmse K, Hubner CA, Isbrandt D, Witte OW, Holthoff K. GABAergic Transmission during Brain Development: Multiple Effects at Multiple Stages. *The Neuroscientist : a review journal bringing neurobiology, neurology and psychiatry* 2017; : 1073858417701382.

9 Bhalla D, Godet B, Druet-Cabanac M, Preux P-M. Etiologies of epilepsy: a comprehensive review. *Expert review of neurotherapeutics* 2011; **11**: 861–76.

10 Cherian A, Thomas S v. Status epilepticus. *Annals of Indian Academy of Neurology* 2009; **12**: 140–53.

11 Tamber MS, Mountz JM. Advances in the diagnosis and treatment of epilepsy. *Seminars in nuclear medicine* 2012; **42**: 371–86.

12 Liigant A, Haldre S, Oun A, *et al.* Seizure disorders in patients with brain tumors. *European neurology* 2001; **45**: 46–51.

13 Karatas H, Gurer G, Pinar A, *et al.* Investigation of HSV-1, HSV-2, CMV, HHV-6 and HHV-8 DNA by real-time PCR in surgical resection materials of epilepsy patients with mesial temporal lobe sclerosis. *Journal of the neurological sciences* 2008; **264**: 151–6.

14 Johnson MR, Sander JWAS. The clinical impact of epilepsy genetics. Journal of Neurology Neurosurgery and Psychiatry. 2001; **70**. DOI:10.1136/jnnp.70.4.428.

15 Gandelman-Marton R, Neufeld MY. Genetic aspects of epilepsy. Harefuah. 2008; **147**. DOI:10.1016/b978-0-409-95022-9.50009-7.

16 Sorge G, Sorge A. Epilepsy and chromosomal abnormalities. Italian journal of pediatrics. 2010; **36**. DOI:10.1186/1824-7288-36-36.

17 Wei F, Yan L-M, Su T, *et al.* Ion Channel Genes and Epilepsy: Functional Alteration, Pathogenic Potential, and Mechanism of Epilepsy. *Neuroscience bulletin* 2017; **33**: 455–77.

18 Kearney JA, Plummer NW, Smith MR, *et al.* A gain-of-function mutation in the sodium channel gene *Scn2a* results in seizures and behavioral abnormalities. *Neuroscience* 2001; **102**: 307–17.

19 Catterall WA. From ionic currents to molecular mechanisms: the structure and function of voltage-gated sodium channels. *Neuron* 2000; **26**: 13–25.

20 Whitaker WR, Clare JJ, Powell AJ, Chen YH, Faull RL, Emson PC. Distribution of voltage-gated sodium channel alpha-subunit and beta-subunit mRNAs in human hippocampal formation, cortex, and cerebellum. *The Journal of comparative neurology* 2000; **422**: 123–39.

21 Meisler MH, Kearney JA. Sodium channel mutations in epilepsy and other neurological disorders. *The Journal of clinical investigation* 2005; **115**: 2010–7.

22 Oliva M, Berkovic SF, Petrou S. Sodium channels and the neurobiology of epilepsy. *Epilepsia* 2012; **53**: 1849–59.

23 Shi X, Yasumoto S, Kurahashi H, *et al.* Clinical spectrum of SCN2A mutations. *Brain & development* 2012; **34**: 541–5.

24 Patino GA, Isom LL. Electrophysiology and beyond: multiple roles of Na+ channel beta subunits in development and disease. *Neuroscience letters* 2010; **486**: 53–9.

25 Trimmer JS, Rhodes KJ. Localization of voltage-gated ion channels in mammalian brain. *Annual review of physiology* 2004; **66**: 477–519.

26 Meisler MH, O'Brien JE, Sharkey LM. Sodium channel gene family: epilepsy mutations, gene interactions and modifier effects. *The Journal of physiology* 2010; **588**: 1841–8.

27 Hu D, Barajas-Martinez H, Nesterenko V v, *et al.* Dual variation in SCN5A and CACNB2b underlies the development of cardiac conduction disease without Brugada syndrome. *Pacing and clinical electrophysiology : PACE* 2010; **33**: 274–85.

28 Westenbroek RE, Merrick DK, Catterall WA. Differential subcellular localization of the RI and RII Na+ channel subtypes in central neurons. *Neuron* 1989; **3**: 695–704.

29 Whitaker WR, Faull RL, Dragunow M, Mee EW, Emson PC, Clare JJ. Changes in the mRNAs encoding voltage-gated sodium channel types II and III in human epileptic hippocampus. *Neuroscience* 2001; **106**: 275–85.

30 Lorincz A, Nusser Z. Molecular identity of dendritic voltage-gated sodium channels. *Science (New York, NY)* 2010; **328**: 906–9.

31 Xu R, Thomas EA, Gazina E v, *et al.* Generalized epilepsy with febrile seizures plus-associated sodium channel beta1 subunit mutations severely reduce beta subunit-mediated modulation of sodium channel function. *Neuroscience* 2007; **148**: 164–74.

32 Xu R, Thomas EA, Jenkins M, *et al.* A childhood epilepsy mutation reveals a role for developmentally regulated splicing of a sodium channel. *Molecular and cellular neurosciences* 2007; **35**: 292–301.

33 Hedrich UBS, Lauxmann S, Lerche H. SCN2A channelopathies: Mechanisms and models. *Epilepsia* 2019; **60**. DOI:10.1111/epi.14731.

34 Liao Y, Deprez L, Maljevic S, *et al.* Molecular correlates of age-dependent seizures in an inherited neonatal-infantile epilepsy. *Brain* 2010; **133**: 1403–14.

35 Yamagata T, Ogiwara I, Mazaki E, Yanagawa Y, Yamakawa K. Nav1.2 is expressed in caudal ganglionic eminence-derived disinhibitory interneurons: Mutually exclusive distributions of Nav1.1 and Nav1.2. *Biochemical and Biophysical Research Communications* 2017; **491**. DOI:10.1016/j.bbrc.2017.08.013.

36 Menezes LFS, Sabiá Júnior EF, Tibery DV, Carneiro L dos A, Schwartz EF. Epilepsy-Related Voltage-Gated Sodium Channelopathies: A Review. Frontiers in Pharmacology. 2020; **11**. DOI:10.3389/fphar.2020.01276.

37 Heyne HO, Artomov M, Battke F, *et al.* Targeted gene sequencing in 6994 individuals with neurodevelopmental disorder with epilepsy. *Genetics in Medicine* 2019; **21**. DOI:10.1038/s41436-019-0531-0.

38 Li Z mei, Chen L xia, Li H. Voltage-gated Sodium Channels and Blockers: An Overview and Where Will They Go? *Current Medical Science* 2019; **39**. DOI:10.1007/s11596-019-2117-0.

39 Escayg A, MacDonald BT, Meisler MH, *et al.* Mutations of SCN1A, encoding a neuronal sodium channel, in two families with GEFS+2. *Nature genetics* 2000; **24**: 343–5.

40 Veeramah KR, O'Brien JE, Meisler MH, *et al.* De novo pathogenic SCN8A mutation identified by whole-genome sequencing of a family quartet affected by infantile epileptic encephalopathy and SUDEP. *American journal of human genetics* 2012; **90**: 502–10.

41 Catterall WA. Sodium channels, inherited epilepsy, and antiepileptic drugs. Annual Review of Pharmacology and Toxicology. 2014; **54**. DOI:10.1146/annurev-pharmtox-011112-140232.

42 Syrbe S, Zhorov BS, Bertsche A, *et al.* Phenotypic variability from benign infantile epilepsy to Ohtahara syndrome associated with a novel mutation in SCN2A. *Molecular Syndromology* 2016; **7**. DOI:10.1159/000447526.

43 Reid CA, Berkovic SF, Petrou S. Mechanisms of human inherited epilepsies. *Progress in neurobiology* 2009; **87**: 41–57.

44 Wolff M, Brunklaus A, Zuberi SM. Phenotypic spectrum and genetics of SCN2A-related disorders, treatment options, and outcomes in epilepsy and beyond. *Epilepsia* 2019; **60**. DOI:10.1111/epi.14935.

45 Sugawara T, Tsurubuchi Y, Agarwala KL, *et al.* A missense mutation of the Na+ channel alpha II subunit gene Na(v)1.2 in a patient with febrile and afebrile seizures causes channel dysfunction. *Proceedings of the National Academy of Sciences of the United States of America* 2001; **98**: 6384–9.

46 Liao Y, Anttonen A-K, Liukkonen E, *et al.* SCN2A mutation associated with neonatal epilepsy, late-onset episodic ataxia, myoclonus, and pain. *Neurology* 2010; **75**: 1454–8.

47 Brunklaus A, Ellis R, Reavey E, Semsarian C, Zuberi SM. Genotype phenotype associations across the voltage-gated sodium channel family. *Journal of Medical Genetics* 2014; **51**. DOI:10.1136/jmedgenet-2014-102608.

48 Berkovic SF, Izzillo P, McMahon JM, *et al.* LGI1 mutations in temporal lobe epilepsies. *Neurology* 2004; **62**: 1115–9.

49 Dilena R, Striano P, Gennaro E, *et al.* Efficacy of sodium channel blockers in SCN2A early infantile epileptic encephalopathy. *Brain and Development* 2017; **39**. DOI:10.1016/j.braindev.2016.10.015.

50 Shmuely S, Sisodiya SM, Gunning WB, Sander JW, Thijs RD. Mortality in Dravet syndrome: A review. *Epilepsy & behavior : E&B* 2016; **64**: 69–74.

51 Bartnik M, Chun-Hui Tsai A, Xia Z, Cheung SW, Stankiewicz P. Disruption of the SCN2A and SCN3A genes in a patient with mental retardation, neurobehavioral and psychiatric abnormalities, and a history of infantile seizures. *Clinical genetics* 2011; **80**: 191–5.

52 Carroll LS, Woolf R, Ibrahim Y, *et al.* Mutation screening of SCN2A in schizophrenia and identification of a novel loss-of-function mutation. *Psychiatric genetics* 2016; **26**: 60–5.

53 Dickinson D, Straub RE, Trampush JW, *et al.* Differential effects of common variants in SCN2A on general cognitive ability, brain physiology, and messenger RNA expression in schizophrenia cases and control individuals. *JAMA psychiatry* 2014; **71**: 647–56.

54 Reynolds C, King MD, Gorman KM. The phenotypic spectrum of SCN2A-related epilepsy. European Journal of Paediatric Neurology. 2020; **24**. DOI:10.1016/j.ejpn.2019.12.016.

55 Li G, Pleasure SJ. The development of hippocampal cellular assemblies. *Wiley interdisciplinary reviews Developmental biology* 2014; **3**: 165–77.

56 Khalaf-Nazzal R, Francis F. Hippocampal development - old and new findings. *Neuroscience* 2013; **248**: 225–42.

57 Lisman JE. Relating hippocampal circuitry to function: recall of memory sequences by reciprocal dentate-CA3 interactions. *Neuron* 1999; **22**: 233–42.

58 Kempermann G, Song H, Gage FH. Neurogenesis in the Adult Hippocampus. Cold Spring Harbor Perspectives in Biology. 2015; **7**. DOI:10.1101/cshperspect.a018812.

59 Spruston N. Pyramidal neurons: dendritic structure and synaptic integration. *Nature reviews Neuroscience* 2008; **9**: 206–21.

60 Steward O. Topographic organization of the projections from the entorhinal area to the hippocampal formation of the rat. *The Journal of comparative neurology* 1976; **167**: 285–314.

61 Chronister RB, DeFrance JF. Organization of projection neurons of the hippocampus. *Experimental neurology* 1979; **66**: 509–23.

62 Hoffman GE, Smith MS, Verbalis JG. c-Fos and related immediate early gene products as markers of activity in neuroendocrine systems. *Frontiers in neuroendocrinology* 1993; **14**: 173–213.

63 Sheng M, Greenberg ME. The regulation and function of c-fos and other immediate early genes in the nervous system. *Neuron* 1990; **4**: 477–85.

64 Kovacs KJ. c-Fos as a transcription factor: a stressful (re)view from a functional map. *Neurochemistry international* 1998; **33**: 287–97.

65 Albright B, Dhaher R, Wang H, *et al.* Progressive neuronal activation accompanies epileptogenesis caused by hippocampal glutamine synthetase inhibition. *Experimental Neurology* 2017; **288**: 122–33.

66 Hoffman GE, Lyo D. Anatomical markers of activity in neuroendocrine systems: are we all “fos-ed out”? *Journal of neuroendocrinology* 2002; **14**: 259–68.

67 Schattling B, Fazeli W, Engeland B, *et al.* Activity of Nav1.2 promotes neurodegeneration in an animal model of multiple sclerosis. *JCI insight* 2016; **1**: e89810.

68 Wirrell E. Review of Dietary treatment of epilepsy. Practical implementation of ketogenic therapy. *The Canadian Journal of Neurological Sciences / Le Journal Canadien Des Sciences Neurologiques* 2013; **40**.

69 Painter MJ, Scher MS, Stein AD, *et al.* Phenobarbital Compared with Phenytoin for the Treatment of Neonatal Seizures. *New England Journal of Medicine* 1999; **341**. DOI:10.1056/nejm199908123410704.

70 Catterall WA, Swanson TM. Structural basis for pharmacology of voltage-gated sodium and calcium channels. Molecular Pharmacology. 2015; **88**. DOI:10.1124/mol.114.097659.

71 Burakgazi E, French JA. Treatment of epilepsy in adults. *Epileptic Disorders* 2016; **18**. DOI:10.1684/epd.2016.0836.

72 Haussler U, Bielefeld L, Froriep UP, Wolfart J, Haas CA. Septotemporal position in the hippocampal formation determines epileptic and neurogenic activity in temporal lobe epilepsy. *Cerebral cortex (New York, NY : 1991)* 2012; **22**: 26–36.

73 Kadar A, Wittmann G, Liposits Z, Fekete C. Improved method for combination of immunocytochemistry and Nissl staining. *Journal of neuroscience methods* 2009; **184**: 115–8.

74 Miller DJ, Balaram P, Young NA, Kaas JH. Three counting methods agree on cell and neuron number in chimpanzee primary visual cortex. *Frontiers in neuroanatomy* 2014; **8**: 36.

75 Marguet SL, Le-Schulte VTQ, Merseburg A, *et al.* Treatment during a vulnerable developmental period rescues a genetic epilepsy. *Nature medicine* 2015; **21**: 1436–44.

76 Saper CB. Unbiased Stereology: Three-Dimensional Measurement in Microscopy by C.V. Howard and M.G. Reed. *Trends in Neurosciences* 1999; **22**. DOI:10.1016/s0166-2236(98)01368-x.

77 You JC, Muralidharan K, Park JW, *et al.* Epigenetic suppression of hippocampal calbindin-D28k by ΔfosB drives seizure-related cognitive deficits. *Nature Medicine* 2017; **23**. DOI:10.1038/nm.4413.

78 Barinka F, Druga R. Calretinin expression in the mammalian neocortex: A review. *Physiological Research* 2010; **59**. DOI:10.33549/physiolres.931930.

79 Irintchev A, Koch M, Needham LK, Maness P, Schachner M. Impairment of sensorimotor gating in mice deficient in the cell adhesion molecule L1 or its close homologue, CHL1. *Brain Research* 2004; **1029**. DOI:10.1016/j.brainres.2004.09.042.

80 Blanchard J, Ugwu SO, Bhardwaj R, Dorr RT. Development and testing of an improved parenteral formulation of phenytoin using 2-hydroxypropyl-β-cyclodextrin. *Pharmaceutical Development and Technology* 2000; **5**. DOI:10.1081/PDT-100100548.

81 Martini A, Torricelli C, Muggetti L, de Ponti R. Use of dehydrated beta-cyclodextrin as pharmaceutical excipient. *Drug Development and Industrial Pharmacy* 1994; **20**. DOI:10.3109/03639049409042644.

82 Grateron L, Cebada-Sanchez S, Marcos P, *et al.* Postnatal development of calcium-binding proteins immunoreactivity (parvalbumin, calbindin, calretinin) in the human entorhinal cortex. In: Journal of Chemical Neuroanatomy. 2003. DOI:10.1016/j.jchemneu.2003.09.005.

83 Berges C, Haberstock H, Fuchs D, *et al.* Proteasome inhibition activates the mitochondrial pathway of apoptosis in human CD4+ T cells. *Journal of Cellular Biochemistry* 2009; **108**. DOI:10.1002/jcb.22325.

84 Shin W, Kweon H, Kang R, *et al.* Scn2a haploinsufficiency in mice suppresses hippocampal neuronal excitability, excitatory synaptic drive, and long-term potentiation, and spatial learning and memory. *Frontiers in Molecular Neuroscience* 2019; **12**. DOI:10.3389/fnmol.2019.00145.

85 Kasahara Y, Ikegaya Y, Koyama R. Neonatal Seizure models to study epileptogenesis. Frontiers in Pharmacology. 2018; **9**. DOI:10.3389/fphar.2018.00385.

86 Demir N, Doğan M, Ylmaz S, Peker E, Bulan K, Tuncer O. A confusing coincidence: Neonatal hypoglycemic seizures and hyperekplexia. *Case Reports in Medicine* 2014; **2014**. DOI:10.1155/2014/595412.

87 Fodor A, Zelena D. The effect of maternal stress activation on the offspring during lactation in light of vasopressin. *The Scientific World Journal* 2014; **2014**. DOI:10.1155/2014/265394.

88 Hui Z, Guang-Yu M, Chong-Tao X, Quan Y, Xiao-Hu X. Phenytoin reverses the chronic stress-induced impairment of memory consolidation for water maze training and depression of LTP in rat hippocampal CA1 region, but does not affect motor activity. *Cognitive Brain Research* 2005; **24**. DOI:10.1016/j.cogbrainres.2005.02.014.

89 Watanabe Y, Gould E, Cameron HA, Daniels DC, McEwen BS. Phenytoin prevents stress- and corticosterone-induced atrophy of CA3 pyramidal neurons. *Hippocampus* 1992; **2**. DOI:10.1002/hipo.450020410.

90 Schneiderman JH, Schwartzkroin PA. Effects of phenytoin on normal activity and on penicillin-induced bursting in the guinea pig hippocampal slice. *Neurology* 1982; **32**. DOI:10.1212/wnl.32.7.730.

91 Witter MP, Doan TP, Jacobsen B, Nilssen ES, Ohara S. Architecture of the entorhinal cortex a review of entorhinal anatomy in rodents with some comparative notes. Frontiers in Systems Neuroscience. 2017; **11**. DOI:10.3389/fnsys.2017.00046.

92 Braak H, Braak E. The human entorhinal cortex: normal morphology and lamina-specific pathology in various diseases. Neuroscience Research. 1992; **15**. DOI:10.1016/0168-0102(92)90014-4.

93 Canto CB, Witter MP. Cellular properties of principal neurons in the rat entorhinal cortex. II. The medial entorhinal cortex. *Hippocampus* 2012; **22**. DOI:10.1002/hipo.20993.

94 Miettinen S, Fusco FR, Yrjänheikki J, *et al.* Spreading depression and focal brain ischemia induce cyclooxygenase-2 in cortical neurons through N-methyl-D-aspartic acid-receptors and phospholipase A2. *Proceedings of the National Academy of Sciences of the United States of America* 1997; **94**. DOI:10.1073/pnas.94.12.6500.

95 Kosel KC, van Hoesen GW, West JR. Olfactory bulb projections to the parahippocampal area of the rat. *Journal of Comparative Neurology* 1981; **198**. DOI:10.1002/cne.901980307.

96 Haberly LB, Price JL. Association and commissural fiber systems of the olfactory cortex of the rat. *The Journal of comparative neurology* 1978; **178**. DOI:10.1002/cne.901780408.

97 Kondo H, Witter MP. Topographic organization of orbitofrontal projections to the parahippocampal region in rats. *Journal of Comparative Neurology* 2014; **522**. DOI:10.1002/cne.23442.

98 Cantó C, Houtkooper RH, Pirinen E, *et al.* The NAD+ precursor nicotinamide riboside enhances oxidative metabolism and protects against high-fat diet-induced obesity. *Cell Metabolism* 2012; **15**. DOI:10.1016/j.cmet.2012.04.022.

99 Caballero-Bleda M, Witter MP. Regional and laminar organization of projections from the presubiculum and parasubiculum to the entorhinal cortex: An anterograde tracing study in the rat. *Journal of Comparative Neurology* 1993; **328**. DOI:10.1002/cne.903280109.

100 Ohara S, Onodera M, Simonsen ØW, *et al.* Intrinsic Projections of Layer Vb Neurons to Layers Va, III, and II in the Lateral and Medial Entorhinal Cortex of the Rat. *Cell Reports* 2018; **24**. DOI:10.1016/j.celrep.2018.06.014.

101 Tang Q, Ebbesen CL, Sanguinetti-Scheck JI, *et al.* Anatomical organization and spatiotemporal firing patterns of layer 3 neurons in the rat medial entorhinal cortex. *Journal of Neuroscience* 2015; **35**. DOI:10.1523/JNEUROSCI.0696-15.2015.

102 Egorov A v., Hamam BN, Fransén E, Hasselmo ME, Alonso AA. Graded persistent activity in entorhinal cortex neurons. *Nature* 2002; **420**. DOI:10.1038/nature01171.

103 Boeijinga PH, Lopes da Silva FH. Differential distribution of β and θ EEG activity in the entorhinal cortex of the cat. *Brain Research* 1988; **448**. DOI:10.1016/0006-8993(88)91264-4.

104 Biella G, de Curtis M. Olfactory inputs activate the medial entorhinal cortex via the hippocampus. *Journal of Neurophysiology* 2000; **83**. DOI:10.1152/jn.2000.83.4.1924.

105 Wolff M, Johannesen KM, Hedrich UBS, *et al.* Genetic and phenotypic heterogeneity suggest therapeutic implications in SCN2A-related disorders. *Brain* 2017; **140**. DOI:10.1093/brain/awx054.

106 Deng W, Aimone JB, Gage FH. New neurons and new memories: how does adult hippocampal neurogenesis affect learning and memory? *Nature reviews Neuroscience* 2010; **11**: 339–50.

107 Workman AD, Charvet CJ, Clancy B, Darlington RB, Finlay BL. Modeling transformations of neurodevelopmental sequences across mammalian species. Journal of Neuroscience. 2013;33(17). doi:10.1523/JNEUROSCI.5746-12.2013

108 Ulrich K, Liu Y, Samehni M, Marguet S, Neves RM, Jakovcevski I, et al. Early postnatal cellular and network perturbations in the hippocampus of mice with a genetic Nav1.2 channelopathy. Abstact649.22, Societey for Neuroscience; 2019. https://www.abstractsonline.com/pp8/#!/7883/presentation/70672

109 Samehni M. Morphological characterization of the hippocampus of neonatal mice carrying the epilepsy mutation Scn2a (A263V) (Unpublished master's thesis). University of Applied Sciences Bonn-Rhein-Sieg.

Attachment

Table of Figures

Table of tables